# Lithological and Geomorphological Indicators of Glacial Genesis in the Upper Quaternary Strata, Nadym River Basin

**Oleg Sizov[1], Anna Volvakh[2], Molodkov A.N.[3], Andrey Vishnevskiy[4], Andrey Soromotin[5], and Evgeny Abakumov[6]**

[1]Oil and Gas Research Institute, Russian Academy of Sciences, Moscow, Russia

[2]Sobolev Institute of Geology and Mineralogy, Siberian Branch of Russian Academy of Sciences, Novosibirsk, Russia

[3]Tallin Technological University, Tallin, Estonia

[4]Novosibirsk State University, Novosibirsk, Russia

[5]Tyumen State University, Tyumen, Russia

[6]Saint-Petersburg State University, Saint Petersburg, Russia

## Abstract

Analyzing the genesis of Quaternary sediments is important for understanding the glaciation history and development of marine sediments in the northern part of the Western Siberia. The problem is relevant since there is no consistent concept of the Quaternary sediments genesis in the north of Western Siberia. Their formation is associated with marine, glacial and interglacial sedimentation conditions. The research objective is to identify the persistent features characterizing the conditions of sedimentation and relief formation using the Nadym river basin as an example. The best method for studying this problem is a comprehensive analysis of the lithological, chronostratigraphic, petrographic and geomorphological studies of the Quaternary sediments upper strata. This study provides data from the analysis of the basic characteristics of quartz grains at the site. The rounding and morphology of the quartz grains provide evidence of possible glacial processing of some of the site strata. A petrographic study of selected boulder samples was performed. Some of them, by the shape and presence of hatching, can be attributed to glacial basins. The first use of a detailed digital elevation model applied to the study area made it possible to identify specific relief forms that could very likely be created during glaciations. Based on the analysis, we propose to consider the vast lake-alluvial plains in the Nadym river basin as periglacial regions. This idea lays the lithological framework for understanding the reasons for the formation of the modern landscape structure. The materials and descriptions provided are of interest to researchers of Quaternary sediments, topography, vegetation, and soil cover; particularly researchers engaged in revising the history of the natural environment development in the north of Western Siberia.

*Keywords: Western Siberia, paleogeography, cover glaciation, Quaternary deposits, quartz grains, petrography, DEM*

## *Introduction*

The history of geomorphological development in the northern part of Western Siberia was a subject of intensive discussion at the end of the 20th century. The stratigraphy of the Yenisey river estuary is a key factor of the West-Siberian lowland quaternary evolution. Numerous examples of sedimentation alternation induced by various cover glaciations of different ages and thicknesses are presented. This series of sediments was used as a background for geological interpretation of the history of Western-Siberian lowland. The Q43 national geological map of Russia for this region indicates the dominance of glacial and fluvioglacial types of the surface sediments (Alyavdin, Mokin, 1957.) The possible existence of ice sheets and related permafrost sediments was identified as a key issue at the beginning of the systematic

geological study of the territory in the 1960s. Some researchers (e.g., Svendsen, 2004) suggested that there were extensive glaciations that resulted in blocking the river or some rivers at certain stages, leading to the formation of large glacier dammed lakes (Grosvald, 1999).

Another point of view considers possible glaciation on the plain (e.g., Generalov, 1986). It explains why the landforms are a sequence of terraces formed by marine transgressions of various ages. There is also an opinion that the glaciation was localized in the form of ice caps on separate watersheds and that the river flow was unblocked (Velichko, 1987; Velichko et al., 1997.) Bolshiyanov (2006) challenged this opinion and introduced the "passive glaciation" concept. In this context, it is assumed that the sea level fluctuations might have created extensive abrasion platforms. Another viewpoint suggests that the forms of relief which previously were considered as glacial and fluvioglacial (morains and easkers), did not originate from cover glaciations, but resulted from erosion, abrasion, and thermokarst outcrops associated with permafrost-erosion and tectonic processes of the late Pleistocene. It was suggested that isolated parts of Smarovskoye glaciation existed in some areas of the Tyumen region combined with relics of ancient marine terraces (Lazukov, 1972) Later, there was a heated discussion in the geology community regarding the nature of possible glaciations and sedimentation history of Western Siberia. It was suggested that glaciations extended up to Siberian ridges that continued as the ancient periglacial Mansyiskoye lake (Grosvald, 1999) Bolshiyanov (2006) suggested that the glaciations were passive, without forming a discontinuous cover or preferential flow blocking in the area topography. At the same time, the abrasion relief with extended ledges was formed in the late Pleistocene period. Finally, the Q-42-43 national geological map suggests that there is a combination of both terrestrial glacial and marine glacial sediments and numerous lake terraces in Western Siberia. Nowadays, the glacial sediments are excluded from the current version of the national geological map (Babushkin, 1995) which in contradicts the results obtained by Astakhov et al. (2016) and Fredin et al. (2012) Currently, there is no uniform concept of the landforms genesis in Western Siberia. The basing of the Nadym River is considered as most important for the Quaternary interpretation of the local Pleistocene history. The topography and sediments of the Nadym River provide the most information for the study of glacial landforms. Many field investigations and remote sensing operations were completed by multiple generations of researchers, providing a valuable baseline for future studies. The results of studying the Nadym River and adjacent areas, combined with other data, served as a basis for a classification of the Quaternary deposits in West Siberia (Maslennikov, 1998, Sedov et al, 2016, Sheinkman et al, 2016, Rusakov et al, 2018.) Nevertheless, the current geological map (Faibusovic, Abakumova, 2015) still has unsolved issues that are highlighted as new geological and geomorphologic data are obtained.

The study objective is to summarize the results of detailed lithological, chronostragraphic, petrographic and geomorphological studies conducted in the Nadym River basin, and to identify the origins of the key factors of sedimentation accumulation and topography.

### *Materials and Methods*

Fieldwork was conducted in 2016-2018 in the Nadym River Basin, including the valleys of its main tributaries: Heigiyaha (Longjugan), Jarudei, Tanlova, Left and Right Hetta. The region is characterized by a moderate human-induced burden. There are main gas pipelines (Urengoy-Pomara-Uzhhorod, Nadim-Punga-Lower Tura, etc.), high-voltage power transmission lines (200, 500 kV), an oil pipeline Yarudeyskoe field CGS to Puryel OPS), and the Nadym-Yagelskoye asphalt road. The survey covered the natural exposures along riverbanks, walls of dry quarries, as well as tops and slopes as the most informative terrain features. The background of this paper is the results of detailed studies of the five most prominent stratigraphy sections of the upper part of quaternary sediments (Figure 1, Table 1.)
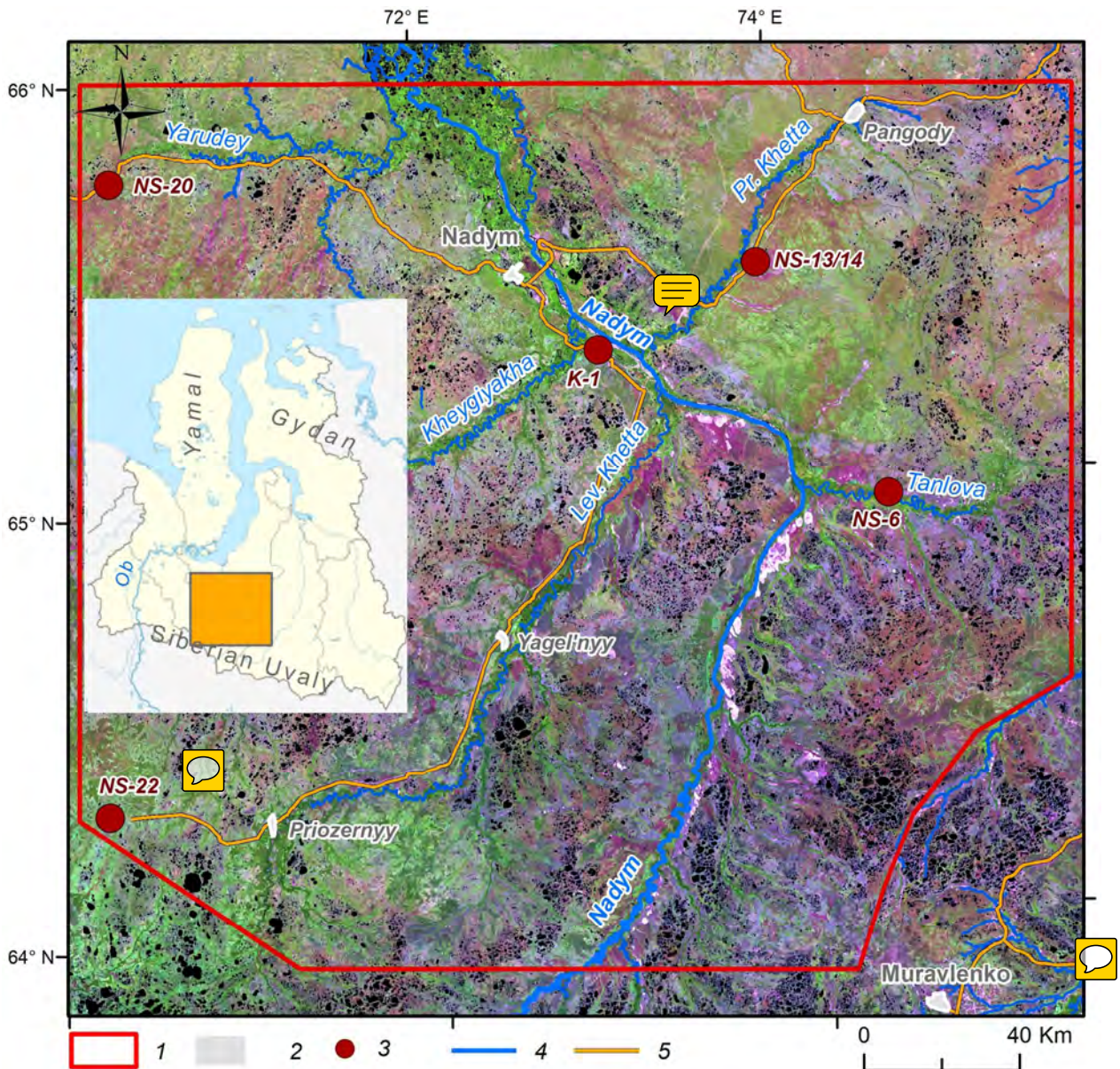
Fig. 1. Overview map: 1: study area; 2: settlements; 3: studied and sampled locations; 4: waterways; 5: roads. Background image: Landsat 8, 2000.

Table 1

Site Properties

| N | Coordinates N, E | Elevation, a.s.l. | Geogenic location | Sampling point location | Survey date | Thickness, m |
|---|---|---|---|---|---|---|
| K-1 | 65.351044 72.974041 | 24 | Second above flood plain terrace | Eall of quarry | 21.08.2016 | 4.2 |
| NS-6 | 64.974808 74.499714 | 44 | Second above flood plain terrace | River break | 18.08.2017 | 9.5 |
| NS -13/14 | 65.52992 73.875985 | 44,5 | Cam sediments | Top and lope of hill | 22.08.2017 | 5.1 |
| NS-20 | 65.778072 70.29182 | 57 | Easker sediments | The wall of quarry | 11.08.2018 | 16 |
| NS-22 | 64.31688 70.232456 | 130 | Watershed | The wall of quarry | 13.08.2018 | 1.5 |

Samples for bulk chemical composition, grain size distribution, sand quartz grain morphoscopy and morphometry, as well as luminescent analysis of sandy textured particles of feldspars were taken from each specified layer of the studied sections in order to clarify the conditions of the sediment formation.

The bulk content of oxides was determined by the X-ray fluorescence method at the Analytical Center for Multi-Elemental and Isotope Research, Siberian Branch (SB), Russian Academy of Sciences (RAS), Novosibirsk, Russia, and at the laboratory of the Institute for Physical, Chemical and Biological Problems of Soil Science (Pushchino, Russia). The grain size distribution was determined by conventional fractions separation (sieve analysis) of samples with the Fritsch Analysette 3 vibratory sieve shaker. The fractions were weighed with laboratory scales, 0.1 g accuracy. 2017 samples were analyzed at the Laboratory of Ground Mechanics, Institute of Cryosphere of the Earth, Tyumen Research Center, Russian Academy of Science with the Mastersizer 3000E laser diffraction particle size analyzer (Malvern Panalytical, Britain).

The Altami CM0870-T binocular microscope was used to study the quartz grains (50 grains per each sample) taken from the coarse sand fraction. The grain surface morphology was studied with the JEOL JSM-6510LV scanning electron microscope (SEM) using the secondary electron image (SEI) at the Analytical Center for Multi-Elemental and Isotope Research, SB, RAS. According to the technique applied (Velichko and Timireva, 1995), the grain scale was determined with L.B. Rukhin pattern (59, Fig. 2) and A. V. Khabakov five-point scale (1946), where 0 is an untreated, and IV is a perfectly rounded grain. The coefficient of roundness and the grade of dullness (Velichko and Timireva, 1995) were estimated for each sample. The dullness of the grains was determined visually as glossy (shiny), quarter-matte, half-matte, and matte. The grain surface microrelief structure study was based on numerous published diagnostic features found in grains with various genesis and sediment accumulation conditions (e.g. Velichko, Timireva, 1995, Krinsley, Doornkamp, 2011; Vos et al., 2014; Woronko, 2016; Kalinska-Nartisa et al., 2017) The previous studies in Western Siberia that examined sand

quartz grain micromorphology covered peat histic sand deposits in the area of Siberian Uvals, valleys of the rivers Taz and Pur, (Velichko et al., 2011) and aeolian sediments of the southern part of Western Siberia (e.g. Sizikova, Zykina, 2015)
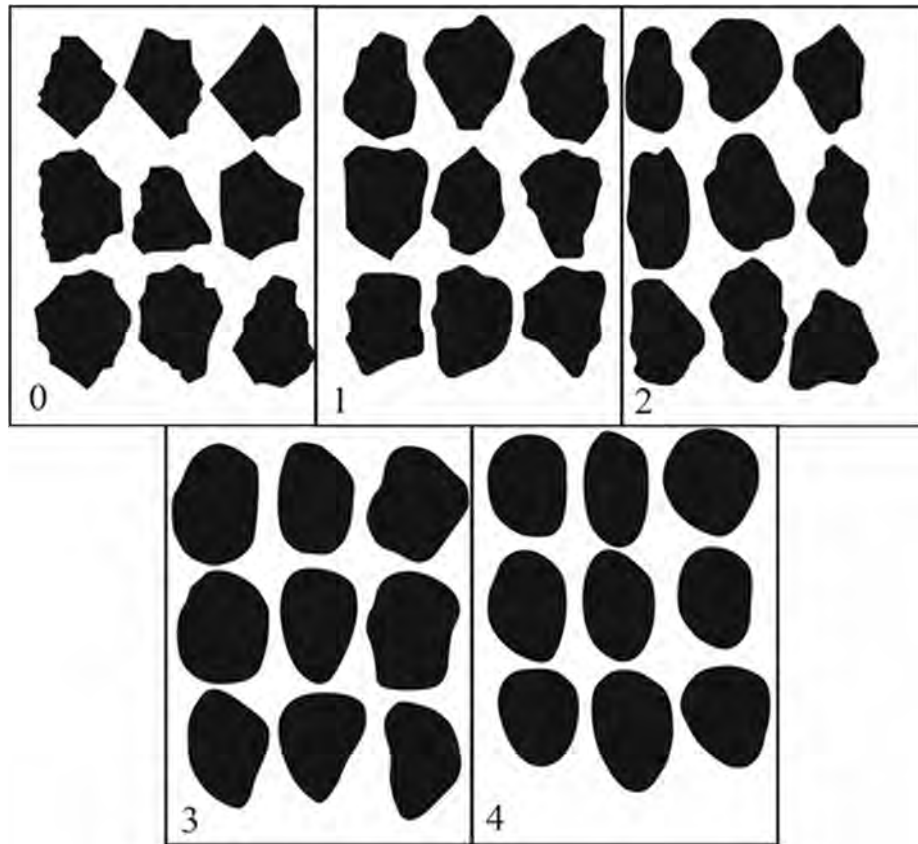
Fig. 2. Pattern for debris scale measurement (Rukhin, 1969)
0, 1, 2, 3, 4 are the classes of roundness (Khabakov, 1946)

The study of potassium feldspar grains, particularly, the determination of the absolute age of the samples, used optically infrared-stimulated (IR-OSL) and thermostimulated (TSL) luminescence (at the Lab of the Quaternary Period Geochronology, Tallinn Technological University headed by A.N. Molodkov) The IR-OSL measurements of the mineral grains extracted from the dating sample were made at the laboratory with a special measurement system having a IR-OSL reader as a primary instrument. The upper limit of the potassium feldspar-based IRSL dating method is normally 300-500 ka, depending on burial conditions and the physical properties of the mineral. The reliability of the dating technique used in this study is demonstrated by several comparative results obtained through both numerical dating methods (K-feldspar-based IRSL, mollusc shell-based electron spin resonance (ESR), quartz-based optically stimulated afterglow (OSA), U-Th, 14C) applied to the same sedimentary samples, and relative ones (Molodkov, 2012) An overview of the IR-OSL dating procedure is presented by Molodkov and Bitinas (2006)

In addition to the analysis at the sampling area, samples were taken for petrographic examination. The samples were cut perpendicular to the lamination or shaleness direction (if any) and made into transparent sections. The Carl Zeiss

172 AxioScope A1 optical microscope at the Geology and Mineralogy Institute, SB
173 RAS (Novosibirsk) was used.
174     For the first time for the studied area, digital terrain models (DTM) with
175 spatial resolution of 12 and 26 m/px based on TerraSAR -X and TanDEM -X radar
176 data were used to characterize the geomorphological structure. Baseline data were
177 obtained from a research project supported by the Terrasar-X research team as part
178 of activities to explore the potential of the TanDEM DTM for research
179 (DEM_GEOL1378.) In addition, public multi-spectrum space images from Sentinel-
180 2 (10 m/px.) were used to clarify the landscape boundaries.
181 (https://scihub.copernicus.eu/.)

182

183     ***Results***

184

185     *Characteristics of the Sections*
186     The summary results of the quaternary sediment section study are shown in
187 Figures 3-7 and Annexes 1, 2. From the data obtained, the following characteristic
188 conditions of sediment accumulation can be distinguished:
189
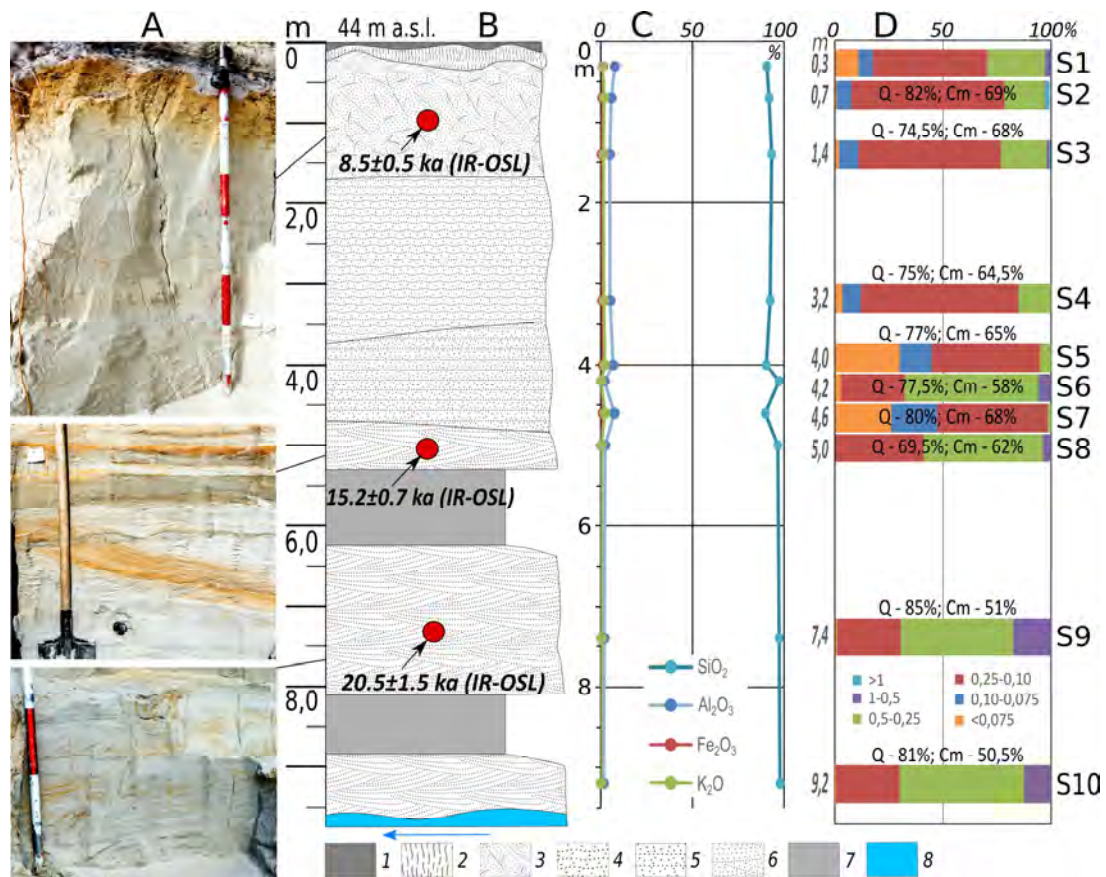
190
191 *Fig. 3. Summary results of research for NS-6 section. A: photographs (Sizov O.S., 2017); B:*
192 *geological structure; C: bulk chemical data; D: grain size distribution (fractions, mm.) Symbols:*
193 *1: podzol horizon of modern soil; 2: illivial-iron (spodic) horizon of modern soil; 3: sands without*
194 *stratification; 4: undulating sand with secondary ironing; 5: horizontally layered sand with*
195 *stratification of loam; 6: medium-and coarse-grained oblique sand; 7: colluvium; 8: river level;*
196 *Q: coefficient of roundness of the sand quartz grains; Cm: degree of dullness; S: sample number.*
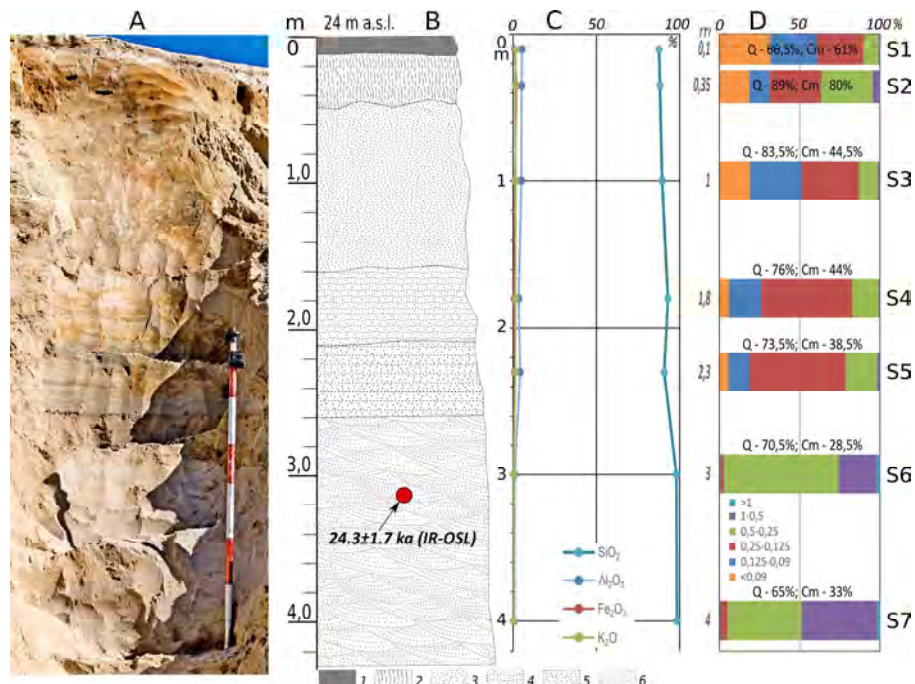
197
198 *Fig. 4. Summary results of research for K-1 section: A: photographs (Sizov O.S., 2017);*
199 *B: geological structure; C: bulk chemical data; D: grain size distribution (fractions, mm.)*
200 *Symbols: 1: podzol horizon of modern soil; 2: illivial-iron (spodic) horizon of modern soil; 3:*
201 *sands without stratification; 4: undulating sand with secondary ironing; 5: horizontally layered*
202 *sand with stratification of loam; 6: medium-and coarse-grained oblique sand; 7: colluvium; 8:*
203 *river level; Q: coefficient of roundness of the sand quartz grains; Cm: degree of dullness;*
204 *S: sample number.*
205
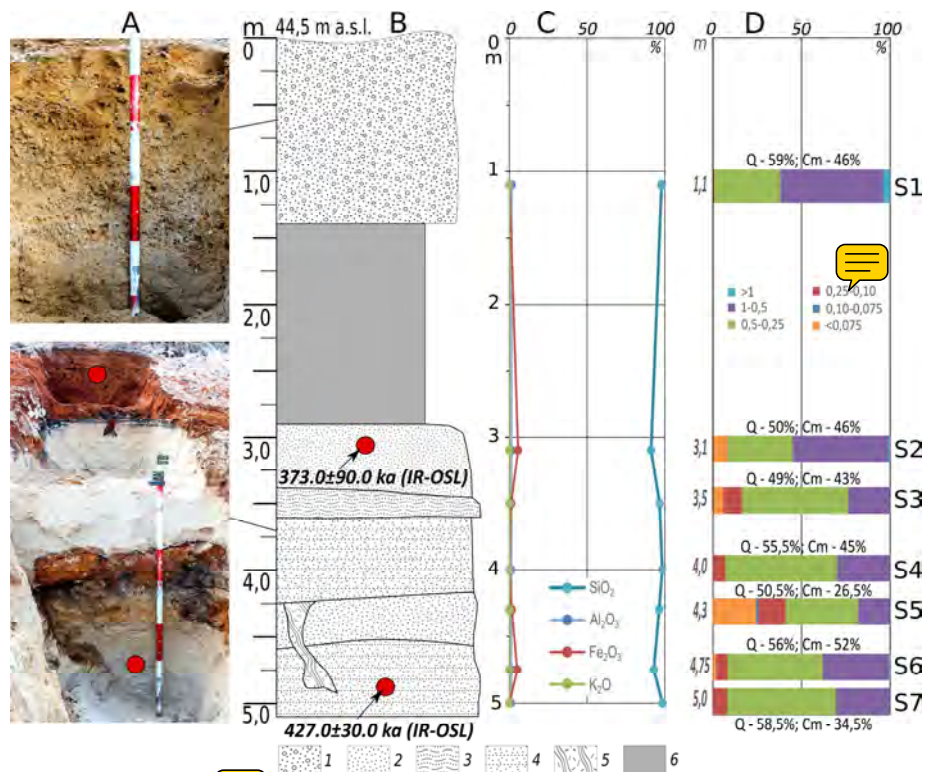
206
207 *Fig. 5. Summary results of research for NS-13/14 section: A: photographs (Sizov O.S.,*
208 *2017); B: geological structure; C: bulk chemical data; D: grain size distribution (fractions,*
209 *mm.) Symbols: 1: coarse sand with pebbles; 2: unstratified red sand; 3: undulating black sand;*
210 *4: horizontally layered sand; 5: wedge filled by deposits of Layer 4; 6: colluviums; Q: coefficient*
211 *of roundness of the sand quartz grain; Cm: degree of dullness; S: sample number.*
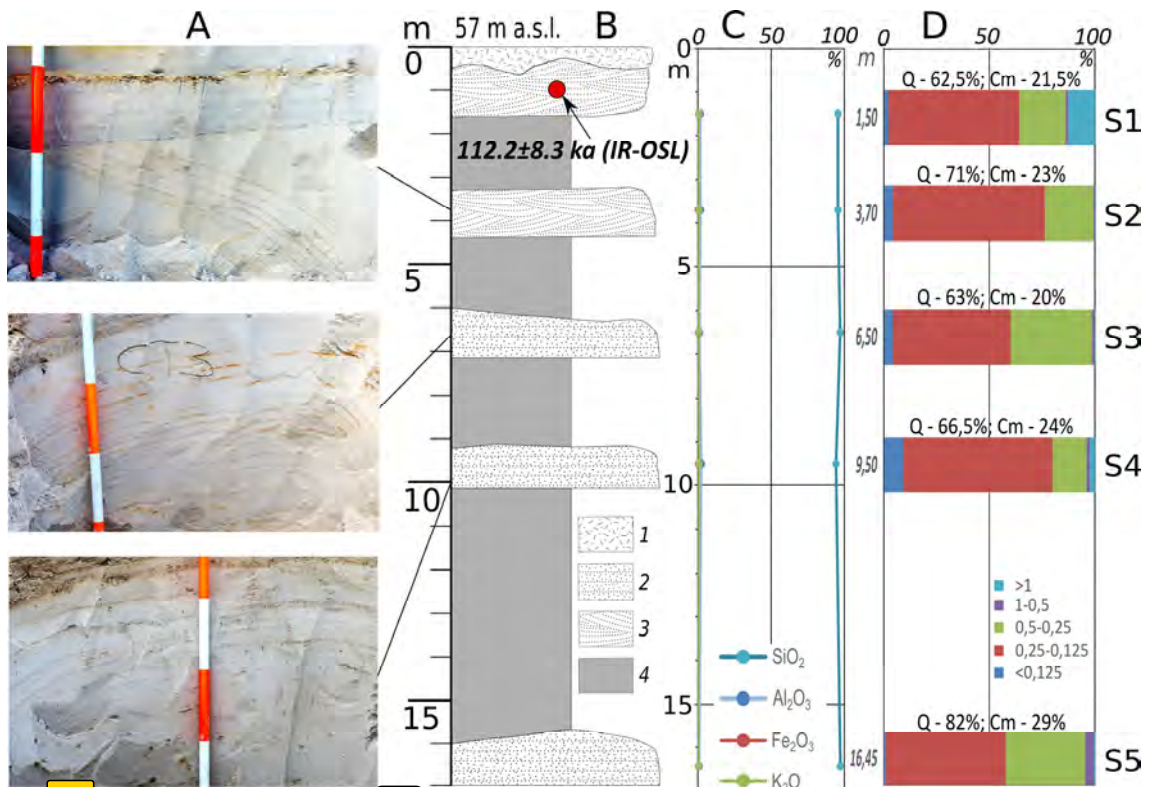
Fig. 6. Summary results of research for section NS-20: A: photographs (Sizov O.S., 2017); B: geological structure; C: bulk chemical data; D: grain size distribution (fractions, mm.) Symbols: 1: overburden; 2: horizontally layered sand; 3: medium-and coarse-grained oblique sand; 4: colluvium; Q: coefficient of roundness of the sand quartz grains; Cm: degree of dullness; S: sample number.
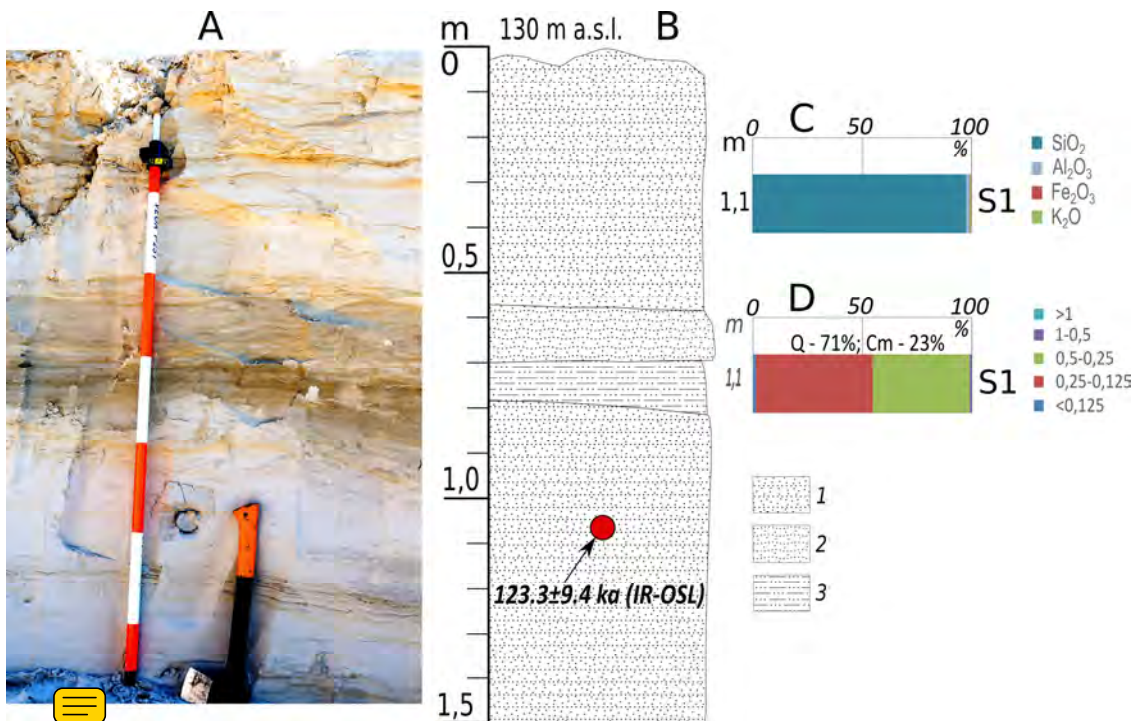
Fig. 7. Summary results of research for section NS-22: A: photographs (Sizov O.S., 2017); B: geological structure; C: bulk chemical data; D: grain size distribution (fractions, mm.) Symbols: 1: horizontally layered grey sand; 2: oblique layered sand; 3: horizontally layered sandy loam; Q: coefficient of roundness of the sand quartz grain; Cm: degree of dullness; S: sample number.

1. Alluvial deposits predominate at the lower geomorphological level (up to 40-45 m.) Sections K-1 and NS-6 show the similar structure of the second above-ground terrace of the Nadym and Tanlov rivers: in the upper part, thick podzolized soil is formed over the aeolian deposits, in the middle part, floodplain type deposits dominate, and in the lower part they are replaced by well-leached gray layered sand. Down the profile, the $SiO_2$ content increases, while the content of other chemical elements is low. The middle part of the section is dominated by fine and medium-grained sand, the portion of large fractions increases in the lower part where single pebbles up to 3-4 cm dia. are found. There are no permafrost-affected sediments.

2. At the middle geomorphological level, the sections show the structure of a NS-13/14 kamiform hill and a linear-oriented relief (NS-20) The top of the hill is covered with a solid layer of pebbles; at 1.2 m depth, it is followed by coarse sand. Sandy deposits forming two distinct cycles are exposed in the middle part of the hill. The unbroken red-colored sand is followed by black sand with slightly horizontal orientation, which in turn is followed by light-grayish horizontally layered sand. In the lower profile, the cycle is repeated; the difference is that the layer of intensively reddish sand is not as thick. In the left lower part of the section, there is a frost wedge microdepression, filled with the rock of layer S4. In general, the section is dominated by medium- and coarse-grained sands of monomineral composition (the shares of Fe, Al and other chemical elements are insignificant.)

In section NS-20, the slope of the extended elevation is exposed. It is composed of a monotonic body of grey monomineral parallel and oblique-oriented quartz sand. The sands throughout the section have an identical grey color and fine-grained composition. The presence of thin ion-containing layers does not affect the chemical composition of sediments: SiO2 prevails in all layers. Local hills up to 5-8 m high covered with large pebbles and boulders on the surface were found on the top of the ridge along the survey path. In an exploration ditch on the top of the microhill (1.5 m deep), large-grained non-grained sandy sediment with the abundance of weakly rolled pebbl gravel, and single large (up to 30-40 cm) boulders were exposed. Their structure is similar to the deposits of the upper part of section NS-13/14. In both sections, permafrost sediments and traces of frost cracking are not found.

3. On the upper watershed geomorphological level NS2, sandy and pebble deposits with the prevailing horizontal orientation were exposed on the flat slope of the eastern cropping of the large local elevation. Sands in the sample are grey-colored, fine and medium-grained. The $SiO_2$ content is 96.49%. A huge number of large, weakly rolled boulders, up to 1.5 m in size, was found in the quarry and on the sandbank of the nearest lake (100 m.)

It should be noted that grey fine, medium- and coarse-grained sands of monomineral quarts composition are present in all sections (except for NS-13/14.) In river terraces, such sands have oblique lamination, while on the watershed theya reoriented horizontally. The sands have no permafrost features, cracking traces and, in general, poor chemical composition. A landscape vegetation feature of such sediments is pine sparse forests, which are able to grow on poor sandy soils with a well-drained hydrologic behavior. Sandy soils lack organic materials and debris of

270 fossil clams, and do not show any salt content. Despite the presence of large debris
271 on the scree slopes; boulders do not occur directly in the sands. Based on
272 morphological, particle size and chemical features we ~~believe~~ that this type of sand
273 sediment could be formed in subaquatic conditions in more severe environments as
274 compared to modern climatic conditions. This is also ~~confrimend~~ by correlation
275 ~~coeffections~~ value – ~~quarts~~ content is negative correlated with key oxides in buls
276 compostion of the fine earth (Annex ~~2~~).
277
278     *Sediments Dating Results*
279     IR-OSL ages for the sediment samples from the sites studied and the related
280 analytical data are listed in Table 2.
281
282 Table 2
283 Absolute dating by the IR-OSL method

| Section | Sampling depth, ~~m~~ | Sample code | Age, ~~years~~ ~~'000~~ | U (ppm) | Th (ppm) | K (%) |
|---|---|---|---|---|---|---|
| K-1 | 3.15 | RLQG 2443-057 | 24.3 ± 1.7 | 0.11 | 0.45 | 0.01 |
| NS-6 | 1.0 | RLQG 2563-019 | 8.5 ± 0.5 | 0.79 | 0.73 | 0.94 |
| NS-6 | 5.0 | RLQG 2564-118 | 15.2 ± 0.7 | 0.01 | 0.00 | 0.14 |
| NS-6 | 7.3 | RLQG 2565-118 | 20.5 ±1.5 | 0.01 | 0.00 | 0.14 |
| NS-13/14 | 3.1 | RLQG 2567-019 | 373.0 ± 90.0 | 0.00 | 0.00 | 0.00 |
| NS-13/14 | 4.9 | RLQG 2568-019 | 427.0 ± 30.0 | 0.35 | 0.74 | 0.00 |
| NS-20 | 1.1 | RLQG 2577-059 | 112.2 ± 8.3 | 0.96 | 4.19 | 0.34 |
| NS-22 | 1.0 | RLQG 2578-059 | 123.3 ± 9.4 | 1.29 | 2.00 | 1.31 |

284
285     From section K-1, a single date of 24.3±1.7 (RLQG 2443-057) was obtained
286 at the depth of 3.2 m. According to this age ~~for the deposits studied there~~, ~~its~~
287 ~~formation~~ took place at the very end of the third ( Lipovka-Novose[]o) warm phase,
288 which was recorded in the north of Western Siberia during MIS 3 by both the [14]C
289 (Kind, 1974) and mollusc shell-based ESR (Molodkov, 2020) methods.
290     The normal sequence of the youngest ages of 20.5 ka (RLQG 2565-118), 15.2
291 ka (RLQG 2564-118), and 8.5 ka (RLQG 2563-~~118~~) was obtained for section NS-6
292 at the depths of 7.3 m, 5 m, and 1 m, respectively. Specific analytical features suggest
293 the supply of the sedimentary rock from the same source area. The genesis of the
294 deposits is also identical. It implies similar conditions for the rock transfer despite
295 the likely difference in climatic conditions.
296     Somewhat unexpected were the dating results for two consecutive layers in
297 section NS-13/14: 427.0 ka (RLQG ~~2567-119~~) and 373.0 ka (RLQG ~~2567-119~~.)
298 Finding very old Pleistocene deposits (MIS 11) is exceedingly rare. Judging from
299 the analytics, the sedimentary rock in these layers came from different source areas
300 and has fluvial, most likely river genesis. Under the given conditions of burial and
301 physical properties of the mineral, the upper dating limit may be at least three times
302 higher (i.e., up to about a million years~~.~~)
303     The last two datings at 123.3 ka (RLQG 2578-~~1~~59) and 112.2 ka
304 (RLQG 2577-~~1~~59) were obtained from two sections: NS-22 and NS-20. They
305 common feature is that both of them fall into MIS 5, as well as the fact that the

corresponding sedimentary rock also came from various source areas. The studied
sediments on the base of a group of key features are supposed to have fluvial (river
and lake) origin.

*Sand Quartz Grain Morphoscopy and Morphometry.*

Refer to Annexes 4-13 for the key results: coefficient of roundnesss, degrees
of dullness, and examples of the quartz grain appearance. The following is a brief
description of the main features.

NS-6. Aeolian genetic group. The upper part of the section (samples S2 and
S3) is characterized by a high coefficient of roundnesss (Q; 74.5 - 82%) and degree
of matting (Cm; 68 - 69%.) $IV^{th}$ rounding class matte grains prevail; the complete
grain distribution vs. rounding and surface dullness are shown in Annex 4. The most
common element of grains microrelief in the S1 sample is a micro-pitted surface
(Annex 9 a, b), which is a feature of aeolian transportation (Velichko, Timireva,
1995.) Chemical etching is sometimes found in depressions. High coefficients of
roundness (Q) and degrees of dullness (Cm) along with the predominance of micro-
pitted grain texture suggest the dominance of aeolian processes during the
sedimentation. Several grains show signs of subaquatic treatment and origin in the
form of crescentic depressions and V-shapes percussions (refer to Annexes 9 a, b),
which preceded the aeolian stage. It seems to be associated with the accumulation
of rock from the river valleys.

For quartz grains from the floodplain deposits (samples S4, S5, S6, S7, S8),
the rounding coefficient (Q) is within the range of 65-80%; the degree of dullness
(Cm) is 58-68% (Fig. 3.) On the average, IV rounding class grains (Refer to Annex
4) with a half-matte surface prevailing in the samples. The number of completely
glossy grains increases (up to 22%.) The entire grain surfaces have signs of
subaquatic processing: V-shaped percussions (Annex 9 d), often forming a fine-
pitted surface (Annex 9 c, d), and separate crescent gouges. Many grains show traces
of aeolian treatment, expressed as a micro-pitted texture (Annex 9 c), which
corresponds well to a sufficiently large share of matte grains in the sample. It can be
assumed that deposits of this layer are formed by fluvial river and aeolian processes
in the coastal environment.

For samples from the lower part of the section (samples S9, S10) Q = 81-85%
and Cm is 50.5-51%. Most grains belong to the IV rounding class. The number of
glossy grains (up to 32%) is significantly higher than in overlying sediments (refer
to Annex 4.) The primary grain treatment traces on the surface of all grains,
regardless of the roundness and dullness, are fine-pitted surfaces (Annex 9 e, f) and
individual well-developed V-shaped microdepressions (Annex 9 f), which is a sign
of active river fluvial transportation. There are grains of the II and III classes of
roundness; they differ from most grains by the presence of flat faces (Annex 9 g, h.)
The shapes of these grains resulted from the previous stages of grain treatment.
There are also signs of aqua treatment on its surfaces (Annex 9 g, h.)
The K-1 grain distribution across the section confirms the primary classification of
the section and matches well the morphometric and morphological properties of the
NS-6 section. Refer to Annex5 for the grain distribution by roundness and dullness.

Layer 6 (samples S6-S7) lying in the base of the section provides important information. These samples differ in grain morphology from overlying sediments. They are characterized by the lowest cross-sectional values of the coefficient of roundness (63-65%) and the degree of mating (33-35%), the presence of glossy grains in all classes of roundness (Annex 10), constrained or ground flat faces at grains, and the development of sickle-like texture and fine pits on the grain surface. With these features, it can be concluded that this layer was formed by fluvial processes, but it should be emphasized that there is a rock in its composition that may have been exposed to glacial processes in the past.

NS-13/14. For S1 deposits Q= 59%, Cm = 46%. Poor-rolled grains, class I (32%) and medium-rounded grains, class II (24%) predominate. Most grains have half-matte (34%) and quarter-matte (32%) surface (Annex 6.) The grains can be categorized into two groups. The first group is represented by well-rounded mature grains with a ubiquitous fine-pitted surface (Annex 11 a), which is a sign of treatment by aqueous streams. In the second group, there are grains of irregular shape (Annex 11 b), often with multiple or conchoidal fractures. The faces have traces of treatment in subaquatic environment. Grains of the second group show separate V-shaped and rarely crescentic-shaped percussions; their number and location indicate a lower exposure to water flow. The presence of these two different groups of grains suggests the ingress of rock from different sources, one of which was the deposits with a poorly treated rock.

For underlying deposits (S2, S3, S4, S5, S6, S7) Q=49 – 58.5%, Cm=26.5-52%.  There, poorly-rounded and middle-rounded grains of classes I and II with a glossy or quarter-matte surface prevail (Annex 6.) The grain surface is dominated by traces of low-activity subaquatic treatment: V-shaped and crescentic microdepressions (Annex 11 c-h.) Irregular grains with smooth surfaces are most common, often with fractures (Annex 11 e, f, h), which probably indicates its arrival from a source with poorly rounded materials. There are grains with conchoidal fractures formed by desquamation processes due to grain freezing (Velichko, Timireva, 1995) or under a big pressure applied to the grain (Immonen et al., 2014; Vos et al., 2014) There are also V-shaped percussions along its surface, suggesting that the deformation occurred before the last fluvial treatment. Many grains were highly exposed to chemical processes expressed as etching through the depressions on the grain and the Fe-Mn skins. The development of V-shaped forms only along the protruding parts of the grain, a well-developed crescentic-shaped texture and non-ubiquitous fine-pits, the average values of the coefficient of roundness and low degrees of maturation suggest that the final processing of grains occurred in a relatively calm aquatic environment. For S2 and S3 samples, in addition to traces of subaquatic treatment, there are grains with small micro-pits (Annex 11 c, d), a sign of aeolian treatment of grains.

NS-20. For samples S1, S2, S3, S4, S5, the coefficient of roundness (Q) is in the range of 62.5-82%, the degree of dullness (Cm) is 20-29%. Glossy grains of II and III classes of roundness prevail (Annex 7.) In the upper sediments (S1), there are signs of aeolian treatment of grains expressed as micro-pits (Annex 12 a, b.) However, they have a rather low value of Cm, which is not typical of aeolian

deposits. This suggests that the local aeolian redeposition of underlying sediments occurred. The underlying layers (S2, S3, S4, S5) have sediment features; their formation is probably associated with fluvioglacial processes: the surface of most grains is highly uneven, cavernous, and strongly mechanically deformed. These properties can be found in glacial conditions (at the stages of previous processing). This is also suggested by the presence of deep-pits, grooves and parallel scratches of various configurations (Annex 12 c, d, h). The last agent in their treatment was a subaquatic process, as indicated by frequently occurring V-shaped and crescentic depressions (Annex 12 e, f, g).

NS22. The coefficient of roundness (Q) is 79%, the degree of dullness (Cm) is 31%. Most of the grains belong to class III of roundness, a slightly smaller number of grains are of class IV; glossy grains prevail (Annex 8). The morphology of the grain surface is quite uniform and is mainly represented by grains with fine pits covering the grain surface almost completely (Annex 13 a-f) or developed only on microelevation parts of the grain (Annex 13 e, f). This surface is a characteristic feature of the long-term grain processing in a sufficiently active subaquatic environment.

*Petrography*

The petrographic analysis of 15 samples taken in a quarry nearby the section AS-3 (fig. 9, coordinates: N65.061417°, E72.943848°) enabled to distinguish several groups of materials:

1) The first group (6 samples) is presented by grey, yellowish-grey, and greenish-grey fine-grained and very fine-grained sandstone and siltstone with slab jointing. They are usually moderately or poorly sorted and have primary foliation that is emphasized by the regular orientation of flattened grains, varying grain size, and matrix content. The matrix is hydromicaceous clay, sometimes with ferruginous cement, with a small portion of silica. The fragments are usually sub-rounded or sub-angular. The rock is composed of polymictic sandstones, similar to arkoses sandstones. Quartz and feldspar prevail among the mineral grains, composing ~30 vol% of the fragments, while another third is predominantly composed of siliceous rock fragments. Some samples contain significant amounts of muscovite (up to 5% by volume), chlorite (including pseudomorphs after the dark-colored minerals), and epidote. The presence of muscovite could be an indicator of low weathering of initial sediments.

2) Pebbles and boulders of the second group of quarzitic and quartz sandstone (6 samples) feature angular forms. The textures are usually massive and vary from poorly to well sorted. The cement is predominantly quartz or quartz-hydromicaceous, sometimes with goethite. The grain size varies greatly, but medium-sized varieties prevail. More than 95% of grains are quartz and siliceous lithoclasts, while muscovite, feldspar, epidote, zircon, monazite, and opaque minerals are also present. The quarzitic sandstones show regenerative incrustations around the primary rounded quartz grains. The grain boundaries are most often irregular and frequently saw-shaped, which indicates a notable meta-genetic alternation. Late veins of the fine-grained quartz aggregate are also rather frequent.

441    3) The third group of samples was the least numerous yet the most
442 informative. In this case, the first sample is a cobble of pinkish quartz trachyte–
443 alkaline intermediate volcanic rock. Large pelletized phenocrysts of potassic
444 feldspar (up to 1 cm) and rare fine quartz grains are distributed in the groundmass
445 composed of pelletized potassic feldspar and quartz (Figure 8(a)). Furthermore,
446 quartz-feldspathic myrmekites are rather frequent. There are small quantities of
447 plagioclase, dark-colored minerals that are substituted by aggregates of chlorite,
448 epidote, and opaque mineral.
449    The second sample is dolerite with typical poikilitic texture (Figure 8(b))
450 formed by large poikilite clinopyroxene crystals (3-4 mm in diameter) with tabular
451 plagioclase (up to 1-1.5 mm.) There are large, separate hypidomorphic crystals of
452 basaltic hornblende (up to 2 mm), which are substituted by hydrous ferric oxides,
453 titanite, and chlorite. The main groundmass contains plagioclase and significant
454 amounts of chlorite, which is presumably a product of substitution of the volcanic
455 glass or clinopyroxene microliths.
456    The third sample is zoisite-amphibolite (zoisite-actinolite) metasomatic rock.
457 Light-green idiomorphic grains of amphibole prevail over hypidomorphic crystals
458 and sheaf-like aggregates of zoisite. Anhedral segregations of titanite and opaque
459 ore minerals are also present. From a general chemical perspective, it can be
460 suggested that the most probable protolith for this rock was a dolerite-like rock.
461
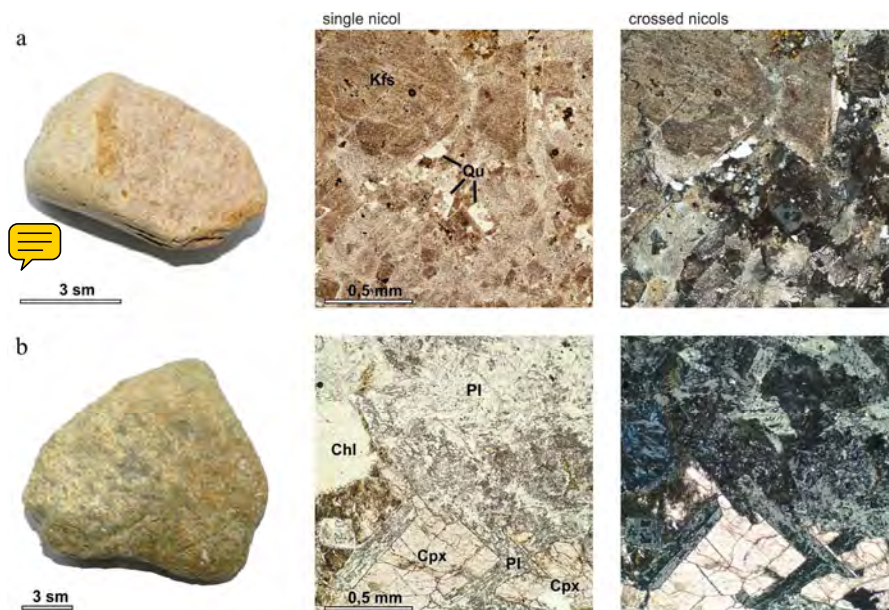
463 Figure 8. (a) Sample N-10 – pinkish quartz trachyte, large inclusions of potassic feldspar (Kfs)
464 with fine quartz grains (Qu) in the quartz-feldspathic matrix; (b) sample N-14: greenish-brown
465 dolerite, large poikilitic clinopyroxene crystals (Cpx) with thin plagioclase crystals (Pl), in the
466 groundmass: plagioclase chlorite (Chl.)
467

468    *Geomorphological Analysis*
469    The investigated area is in the zone of sparse northern taiga with extensive
470 peatlands. Therefore, the existing digital surface model (DSM), based on X-band
471 radar data with high penetration capacity, reflects in detail the terrain structure of
472 the territory. Based on the remote features available in the literature (Atkinson et al.,

473 2014; Astakhov et al., 2016) the DEM mapping of the glacial ice and fluvioglacial
474 relief features was performed using a site with an area of 54,117 ~~sq. km~~ as an
475 example. Its boundaries run along the watershed of the Nadym River and its
476 tributaries. The summary mapping results are shown in Figure 9 and Table 3.
477
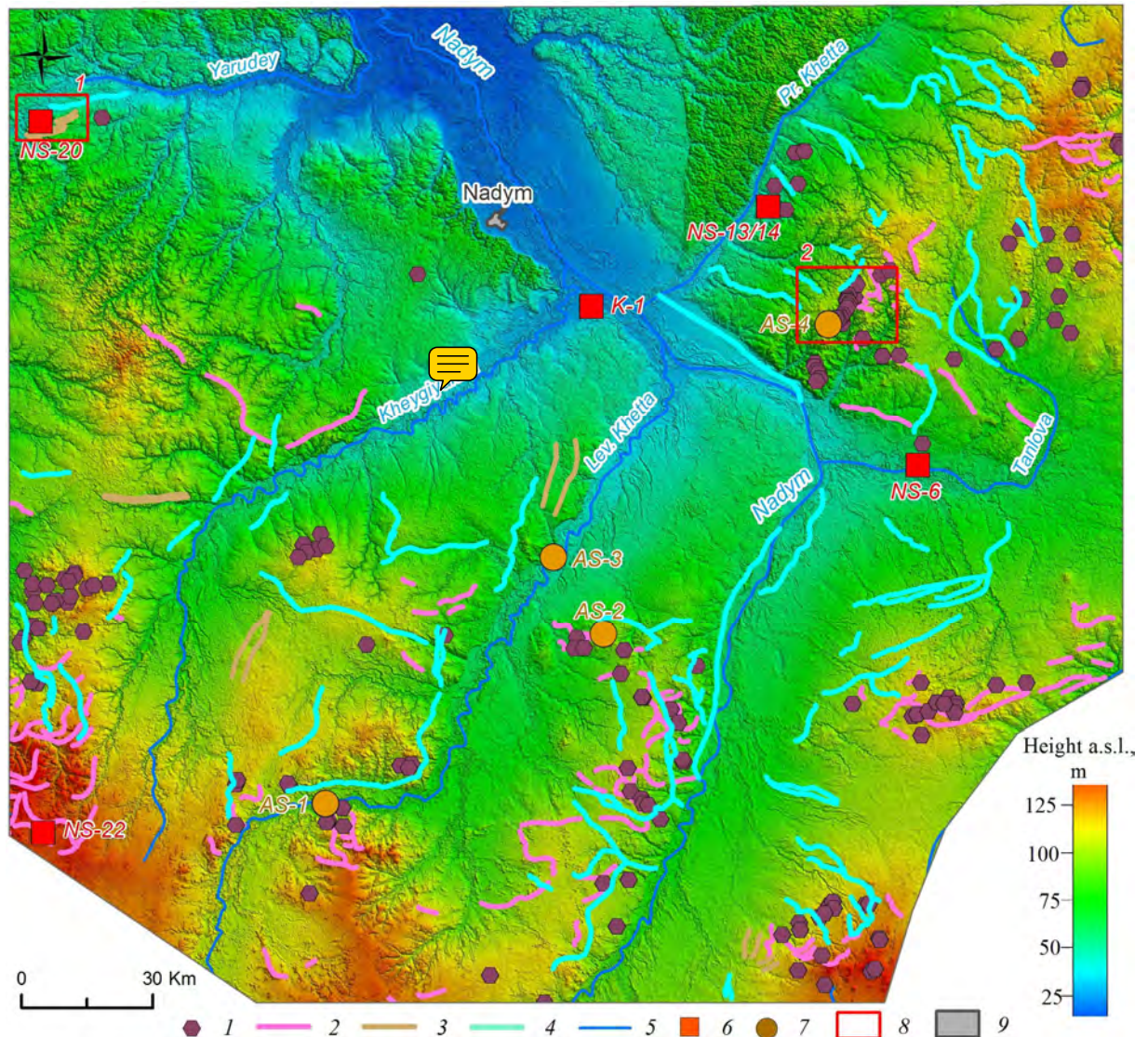
478
479 Fig. 9. Results of the glacial and fluvioglacial relief interpretation in the middle **course** of the
480 Nadym River (the background image is a synthesized digital terrain model based on DEM
481 TanDEM-X, 26 m resolution): *1: kame-like hummocks; 2: moraines; 3: parallel ridges; 4: valley*
482 *trains; 5: waterways; 6: studied and sampled locations; 7: additional locations based on*
483 *Khlebnikov, 1954; Yevseyev, 1958; 9: settlements*

484
485 Table 3
486 Remote mapping of the glacial and fluvioglacial relief features in the Nadym River basin (mid and
487 lower courses)

| Relief features | Number of identified objects | Total area/length, km |
|---|---|---|
| Kame-like hummocks | 157 | - |
| End moraines | 122 | 851.3 |
| Parallel ridges | 16 | 157.2 |
| Valley trains | 103 | 1411.3 |

488

Based on the map obtained (Figure 9), it can be noted that the spread of the assumed glacial and fluvioglacial relief features within the investigated area has two distinct patterns:

– all identified features are to the south off the Jarudei and Pravaya Hetta rivers, with individual objects found in the watershed between Jarudei and Heigiyahi (Longjugan.) In the southern and western parts, the diversity and density of the features are the highest (Tanlova and Pravaya Hetta rivers watershed, left bank of the Nadym River in its middle course)

– all identified features are found at the heights from 40 m a.s.l.. and higher; the density of objects significantly increases in the watershed areas above 70-75 m.

The feature of the high elevation relief distribution is demonstrated by the statistical data about the selected kameform hills. Among the 157 point objects, 145 (92%) are above 75 m, with 53 (34%) located within the narrow range of 95-104 m. Below 75 m, large objects occur individually and are poorly distinguished morphologically.

The network of extended (more than 850 km) proximal (kame) moraines that mark the final glacial massif positions is confidently recognized. They have different stretches (sub-latitudinal, north-western, etc.), which may indicate there was no single direction of cover glacial movement. In most cases, the moraines are confined to the watersheds, while they are often accompanied by other glacial forms (kames, postglacial rills, etc.) The chain of kame hills on the watershed of the Tanlova and Pravaya Hetta Rivers are erosive remnants of the local moraine formations, i.e. morphologically they occupy an intermediate position between the individual moraines. On the watersheds, well-drained, dry areas of sand sands near kame ridges are often subjected to deflation and active redispersal.

Some of the individual objects are linear ridges (about 157 km total length.) The linear ridge relief also has visible signs of erosion (scours, rills, subsidences) and in most cases can be traced as a specific linear landscape texture.

The valleys and rills of the melt glacial waters flow are more than 1,400 km long. The valleys are well expressed in the southern and eastern parts of the study area and are barely visible below 40 m asl. The network of valleys does not really match the modern watercourses; they can be located both in parallel at a small distance from the ancient valleys, or intersect them at right angles. The valleys and hollows of the ancient runoff are often associated with terminal formations. The preservation of valleys is one of the key signs of marine transgression absent in the middle course of the Nadym River since the last glaciation of the region.

For clar, two sections of typically glacial landforms are highlighted on the map (Fig. 5):

1. A site with a predominant linear ridge relief, located on the right bank of the Yarudey River (left tributary of the Nadym River), near the Nadym-Salekhard highway under construction (Fig. 10.) Four long, curved ridges reaching a height of 55 m are well-preserved (the difference in relative heights is 10-12 m.) To the south of the ridges stands a section of hilly, presumably kame, relief. The ridges are complicated by thermokarst and erosion features.

533  2. The kame hill concentration site on the right bank of the Nadym River, south of the main gas pipelines (Fig. 11.) The kames reach an absolute height of more than 100 m (difference in relative height up to 30 m.) The kames are well preserved despite the destruction of individual features by the river erosion.
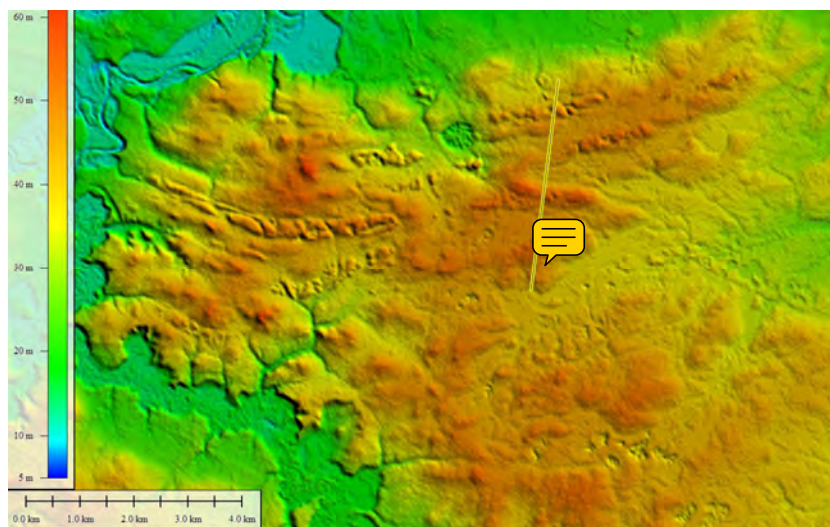
*Fig. 10. Parallel ridges, DEM TanDEM-X, 12 m / pixel*
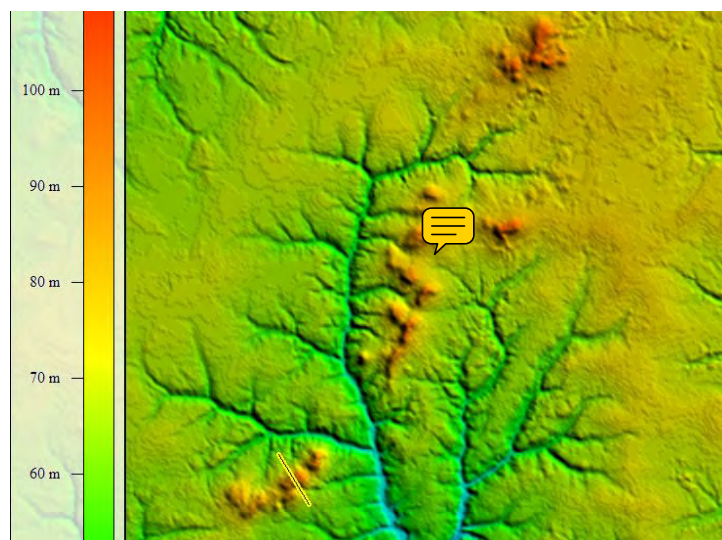
*Fig. 11. Kame-like features, DEM TanDEM-X, 12 m / pixel.*

***Discussion***

According to current viewpoints, the territory of the north of Western Siberia was exposed to several cover glaciations: Zyryanka (MIS4), Taz (MIS6) and Samarovo (MIS8.) Areas at the lower level (up to 40-45 m a.s.l.) could represent serial repeated marine transgressions in Kazantsev (MIS5) and Karga (MIS3) ages. The glaciation boundary is presented in Figure 12, the chronological match of the Western Siberian glaciation to the interglacial periods of the Eastern European glaciation is presented in Figure 13. Directly within the boundaries of the investigated areas, numerous researchers identified the boundaries of MIS6 stages of Taz (MIS4) and possibly Zyryanka glaciation periods.
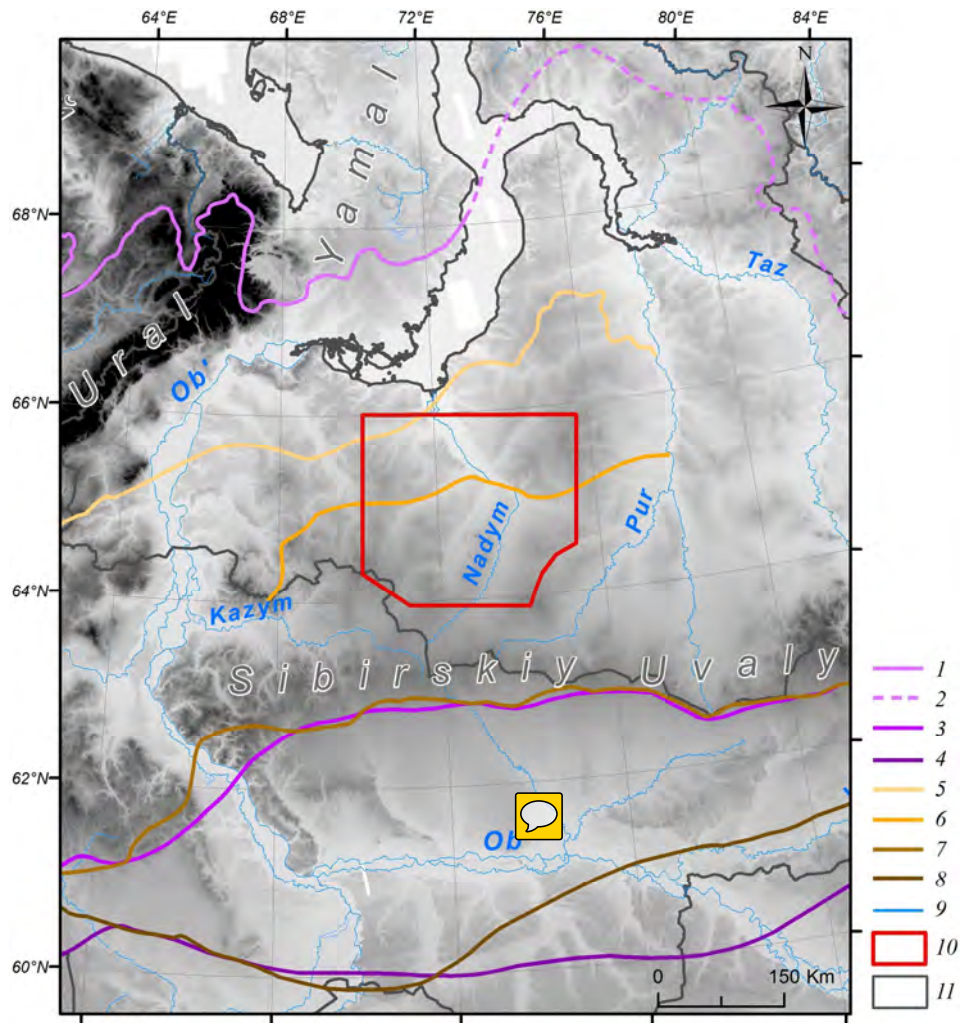
Fig. 12. 1-8: ice sheet boundaries (1: Zyryanka (Astakhov et al., 2016); 2: Zyryanka (assumed) (Astakhov et al., 2016); 3: Taz (Astakhov et al., 2016); 4: Samarovo (maximum) (Astakhov et al., 2016); 5: Zyryanka (Zemtsov, 1976; Babushkin, 1996); 6: Taz (second stage) (Zemtsov, 1976; Babushkin, 1996); 7: Taz (Zemtsov, 1976); 8: Samarovo (Zemtsov, 1976)); 9: water bodies; 10: study area; 11: administrative boundaries

Рис. 13. Palaeoenvironmental event successions on the East-European Plain (from Bolikhovskaya, 2004; Molodkov and Bolikhovskaya, 2010) and in Western Siberia (Interregional Stratigraphic Chart..., 2014.)

The key natural feature of the glacial genesis of quaternary strata in northern Western Siberia is the presence of wrecked rock: semi-rounded angular stones, gravel and large boulders with evident glacial hatching, carried over by the glacier from the territories outside the West Siberian Plain (Strelkov et al., 1965; Zemtsov, 1976). The water-glacial sediments in the research area include well-washed grey sand characterized by poor chemical composition (the gravimetric concentration of $SiO_2$ is 94-97%) and also containing amendments of gravel and stones (Chekunova, 1954; Groysman, 1954; Khlebnikov, 1954). The glacial sediments include unsorted coarse-grained sands with an abundance of pebbles, as well as moraine-like bodies of lumped clay, loam, and clay sand with gravel and large boulders. The petrographic composition of boulders and pebbles includes quartz, opal, sandstones, quartz porphyres, amphibolites, granitoids, gneisses, trachites, etc. (Chekunova, 1954; Groysman, 1954; Khlebnikov, 1954). However, it was noted that interpreting the exact location of the origin of these rocks from the geological markers representing different territories is so far problematic.

The results of the study of the sections, in general, showed that the youngest of the discussed sediments are those of the second floodplain terrace (section NS-6, K-1). In the top part, it includes aeolian sand formed no later than the beginning of the Holocene (MIS1), in the middle part there are floodplain series of alluvium, in the lower part there are river streams of grey oblique sand of the late MIS3 - middle MIS 2.

The absolute age of the second floodplain terrace formation of the Nadym and Tanlova Rivers (sections K-1 and NS-6) correlates well with numerous radiocarbon and OSL datings of the second terrace throughout all the northern Western Siberia (the age ranging from 42,000 to 25,000 years) (Nazarov, 2015). On average, the age of the cover formation is between 20,000 and 12,000 years (Zemtsov, 1976; Astakhov, 2006). Two types of glacial relief areas and extensive sandur surfaces were identified on the surface of the second floodplain terrace in the large-scale field studies on the left bank of the Left Kheta River (Vasilyev, 2007).

At the middle and upper geomorphological level, grey monomineral sand with a similar age at the beginning of the NS-20 stage was also found in the NS-22 and MIS5 sections. It can be suggested that during the Kazantsev interglacial period in the vast area of the Nadym River basin there were favorable conditions for the erosion of the previously accumulated sandy textured deposits and their transfer downstream the main rivers.

One of the most interesting points of research is the kameform hill on the left bank of the Right Hetta River (NS-13/14), the formation of its middle part corresponds to the Tobol interglacial period (MIS9-11). It can be suggested that the sediments in the upper part of the hill are not younger than the Taz glaciation (MIS6), while the pebble layer formed during the degradation of the glacier reinforced the previous sediments and later was resistant to erosion, and was not covered by the waters of the Kazantsev and Karga transgressions

The results of the sand quartz grain morphology analysis confirmed the supposed genesis of the studied sections. Thus, for sections NS-6, K-1 it was shown that in the upper part of sections there are aeolian sediments, below is floodplain

sand followed by fluvial sand. At the base of both sections, there are sediments in which, apart from typically river grains, a large number of various morphology grains are found. These are grains of varying degree of roundness, irregular shape with a smooth surface and smooth faces, often on their surface, there are various grooves and scratches formed under the strong mechanical impact, as well as conchoidal fractures. Their origin could be a result of freezing weathering and cryogenic transformation (Velichko, Timireva, 1975), as well as of high pressure applied to the grain surface (Vos et al., 2014; Immonen et al., 2014.) Well-rounded ellipsoid and ball-shaped grains predominate in the top layer sediments. One can associate this distribution with materials coming from two different sources. One source could have been the former glacial sediments eroded by fluvial processes. This type of terrace structure corresponds well with the results of the study by Velichko et al. (2011) who analyzed sands with underlay peat deposits in the investigated region.

Quartz grains from sections NS13/14 and NS20 are often characterized by low rounding classes, multiple conchoidal fractures, sometimes even conchoidal systems, a deep-pitted surface, scratches, grooves, and cleavage surfaces. Such elements could be signs of processes that occur in glacial environments. Often, there are also signs of subsequent water treatment: separate crescentic depressions and smoothed sharp peaks of grains. It indicates the redeposition of the glacial grains by water flows. Along with the grains described above, there are also typical subaquatic grains: well-rounded with a fine-pitted surface, but their number is inferior to grains with glacial features.

Currently, we lack sufficient evidence to confirm the glacial genesis of these deposits. It is possible that the grains were exposed to the effects of glacial processes, with a final processing phase in their history that included subaquatic processes. In section NS-22, the grain morphology provides evidence that suggests the existence of a quiet subaquatic environment under which quartz grains underwent long-term treatment.

In general, the results of sand quartz grain morphoscopy and morphometry show that most quartz grains from all sections underwent complex multi-stage processing throughout their life.

The petrographic diversity of erratic boulders in West Siberia helps us distinguish two or three paleoglacial regions that combine several dozen distributed provinces. Each is characterized by a specific set of rocks and petrographic features. The first major generalization in this respect was made by Zemtsov (1976), who identified the guide boulders of the Ural region as ultramafic and mafic rocks of the Main (axial) Uralian zone, plagio-granites, and highly metamorphosed rocks (gneisses and shales.) In the Central Siberian region, the prevailing boulders include dolerites and basalts of the Putorana Plateau, as well as various granitoids, quartzites, and Palaeozoic sandstones of the Taimyr Region. These studies were substantially supplemented and detailed by a much more ambitious work by Sukhorukova et al. (1987.)

Despite their small quantity, the petrographic analysis of pebbles and boulders led to the following conclusions. First, high-silica alkaline effusive rocks (sample

656 N-10, quartz trachyte) are indicative of both the Northern Taimyr Province (Troitsky
657 & Shumilova, 1973) and many moraines of the Ural paleoglacial region
658 (Sukhorukova et al., 1987), but they are never found in the Putorana Plateau and the
659 southmost regions. Moreover, there is only a small relative share of dolerites (sample
660 N-14, dolerite) and other effusive mafic rocks, which is a property of Putorana and
661 Nizhnyaya Tunguska regions. In contrast, there is no limestone that would be typical
662 of the Central Siberian paleoglacial region (Kulyumbinsk and Sukhaya Tunguska
663 distributive provinces according to Sukhorukova et al., 1987.) However, there is no
664 granite in the samples either, which is a property of the Northern Taimyr region.
665 Second, quartz and quartzite sandstones are typical for the Ural paleoglacial
666 region, but their share is usually within a few per cent. Quartzitic sandstones also
667 described as Palaeozoic were found 50 km north of Surgut within the tentative
668 Central Siberian and Middle rock outwash zones (Sukhorukova et al., 1987.) The
669 source of the polymictic platy jointing sandstone could be the Palaeozoic bordering
670 of the eastern slope of the Urals (Sukhorukova et al., 1987) or the Mesozoic
671 sandstone of the West Siberian Plate.
672 In general, the samples have a significant proportion of terrigenous rocks
673 (sandstones and siltstones) and low content of dolerites. On the one hand, this can
674 be explained by the poor representativeness of the samples. Nevertheless, the key
675 washout zone could be located further north than the Putorana Plateau in the Taimyr
676 area. To substantiate this point of view, further research is planned to determine the
677 trace element composition and absolute dating and to expand the sampling.
678 Despite the numerous features that make it possible to attribute the thickness
679 of grey monomineral quarts sand (K-1, NS-6, NS-20) to fluvioglacional sediments,
680 and the upper pebble strata of section NS-13/14 to glacial sediments, the study did
681 not find typical moraine-like formations of lumped clay, loam and clay sand with
682 gravel and large boulders in this territory. However, detailed descriptions of this type
683 of sediment can be found in some references.
684 Thus, in the middle course of the Right Hetta River at Point 70 (Khlebnikov,
685 1954) 2.5 m deep there is a 20-meter layer of densely clumped loam with interlayers
686 of mica enriched sand (the layers are up to 20 cm wide) (section AS-1, Fig. 9.) The
687 color of the loam is brown-reddish-brown, small glitter mica is visible, and small
688 corners of debris (granite) are found, up to 25 cm in diameter. In the right part of the
689 section upstream, stripping exposed a layer of fine-grained sand. Below 15 m it is
690 followed by an interlayer of gravel-pebble rock. The prominent colluvium slope is
691 covered by loam crushed stone, and a cluster of gravel-pebble rock is also found on
692 the beaker. The huge kame moraine was described in the watershed of Nadym and
693 Levaya Hetta rivers (point 2368) (section AS-2, fig. 9) (Khlebnikov, 1954).
694 It has a wide extension and rises up to 25-30 m above the surrounding plain.
695 The ridge part of the range is convex and consists of individual peaks separated by
696 meso ridges. On the surface of the ridge, the congestion of pebble and gravel is
697 found. The gravel-pebble coarse-grained well-washed and leached sand is traced
698 down to the depth of 1.2 m.
699 Two esker-like linear elevations and a small kameform hill were discovered
700 in the lower course of the Right Hetta River at well No. 18 (Khlebnikov, 1954) at

1.8 m depth in the gravel-pebble horizon with a total depth of 17.6 m (section AS-3, Fig. 9.) The diameters of the pebbles are between 0.5 and 3-4 cm. The pebbles are not rolled and consist mainly of quartz and sandstone.

The moraine hills in the upper part of the Bolshoy Huhu River (right tributary of the Nadym River) have a north-west and a north-east orientation. The length reaches 6-7 km, and the relative height varies from 15 to 60 m. (Chekunova, 1954; Yevseyev, 1958) morphologically, the steep slopes of the hills have individual smoothed tops separated by small saddles. The upper layer of the hills to a depth of 1-2 m is peeled loam with abundant pebble rock. The pebbles are weak and poorly rolled, and their diameters do not exceed 2-4 cm. Petrographic composition in one of the sections reveals (so-called point 367 (Chekunova, 1954): silica, clay shale, arkoses sandstones, breccia of clay-quarts rocks and limonite. The results of manual drilling at some small hills (Yevseyev, 1958) (Yevseyev, 1958; Andreev, 1960) showed that they are folded with permafrost sediments. The total ice content as determined visually is not less than 30%. As an example, well No. 10 (Yevseyev, 1958), where light grey clay with yellowish color, light, porous, with alevrite interlayers is found at a depth of 1.4-10.7 m, has a wavy and horizontal lamination (section AS-4, Figure 9.) Clay thickness is underlayed with grey clay fine-grained sands with poor sorting and admixture of gravel grains, quartz, and silicon pebbles.

Data from both our studies and previous field studies are in good correspondence to the results of the analyses with the Tandem-X Digital Terrain Models. These models revealed that despite the plain origin of the territory, the high salinity and dominance of erosion processes, various glacial and fluvioglacial relief features preserved to various degrees (kameform hills, proximal moraines, and linear elevations, glacial meltwaters etc.) are evident.

A linear-oriented relief caused by a glacial impact in northern Western Siberia is highlighted on the Map of Quaternary Formations in Russia, 1:2,500,000 scale (Astakhov, 2016.) At the same time, linear features and glacial remains are identified on geological maps of larger scales (Babushkin, 1995.)

Nowadays, due to the increasing availability of initial DTM data, remote mapping of glacial relief features become the standard method across the world (Clark, 2004; Glasser, 2008; Sharpe, 2010; Atkinson, 2014; the Geological Surveys in Canada and the United States, Norris, 2017.) Based on modern spatial data, a detailed map for the British Isles Territory and Coastal Zone (BRITICE-2) is available for digital study and analysis, and was updated (The BRITICE, 2017.) The remote features of most forms of glacial relief for various natural conditions are described in detail and offer numerous evidence that can be used as standards for remote sensing data interpretation, including the entire north area of Western Siberia.

### *Conclusions*

Our results showed high efficiency of simultaneous application of field ground and remote methods even with limited raw site rocks. Sediments were identified, which can be immediately attributed to fluvioglacial (lower part of section K-1 and NS-6, section NS-20) and glacial (upper layer of section NS-13/14)

origins. Traces of glacial treatment were also found as landforms in certain areas such as kameform hills, proximal moraines, linear-bed elevations and depressions of melt glacial water runoffs. Due to low organic substance content, sparse lichen-pine trees are formed over the fluvioglacial sediments on the low-fertile podzolic soils. It is a characteristic landscape feature of the leaching soil condition for the north taiga in Western Siberia. At the same time, the moraine-like layers of aggregated clay, loam and clay sand with gravel and large stone boulders that could not be found in field studies are widely described in stock sources previously unpublished (particularly the Lion River Basin, Hetta and in the upper reaches of the Great Huhu River.)

Thus, the development history of the Nadym River lower stream area provides evidence that periods of cover glaciations occurred here in the Pleistocene. At the same time, it is difficult to say whether it was a single glacier with a common front, or whether there were several separate centers of ice accumulation. The available data, especially the structure and functional characteristics of the relief, appear to favor the second option, at least in the late Pleistocene. In the early periods, traces of larger glaciation may represent the vast lake-alluvial plains and flood plains, reaching a maximum area in the basin of the Nadym, Pur and Taz rivers. In this case, they can be considered as the latest erosion formations but preserved a characteristic structure inherited by modern landscapes.

### *Acknowledgments*

The authors thank the Terrasar-X (DLR) research team for providing the digital elevation models.

This study was funded by the RFBR and the Local Government of the Yamal-Nenets Autonomous District, project No. 19-45-890008. The investigation is under a public assignment by the Institute of Geology and Mineralogy, Siberian Branch, Russian Academy of Sciences.

### *References*

Alyavdin F.A., and Mokin N.P.: Geological map. 1rd ed. Scale 1:1,000,000. Ministry of Geology and Subsoil Protection of the USSR, Map Q-43 (Novyy Port.) Gosgeoltekhizdat, Moscow, 1957.

Andreev Yu.F. About the relationship of linear-ridge topography with tectonic structures in the north of Western Siberia (in the field of permafrost development.) Geologiya i geokhimiya. Geology and geochemistry, 3(IX), 76–94, 1960.

Astakhov, V.I.: On chronostratigraphic units of the Upper Pleistocene in Siberia, Geologiya i geofizika, 47(11), 1207–1220, 2006.

Astakhov V. Shkatova V., Zastrozhnov, A. and Chuyko, M.: Glacio-morphological Map of the Russian Federation, Quaternary International, 420, 4–14, 2016.

Atkinson, N., Utting, D., and Pawley, S.: Landform signature of the Laurentide and Cordilleran ice sheets across Alberta during the last glaciation. Canadian Journal of Earth Sciences, 51(12), 1067-1083, doi: 10.1139/cjes-2014-0112, 2014

Babushkin, A.E.: Quaternary map. 2rd ed. Scale 1:1,000,000. Russian Federation Committee on Geology and Mining (Roskomnedra), Map Q-42,43 (Salekhard.) St. Petersburg: VSEGEI Cartographic Factory, 1996.

Bolshiyanov, D.Yu.: Passive Glaciation of the Arctic and Antarctic Regions. AANII, Saint

Petersburg, 296 p, 2006.

Chekunova, V.S.: Geological and geomorphological survey of a part of the lower reaches of the Nadym River basin and parts of the right bank of the Nadym Ob River. VSEGEI, Leningrad, 1954.

Clark, C, Evans, D, Khatwa, A., Bradwell, T., Jordan, C., Marsh, S., Mitchell, W., and Bateman, M.: Map and GIS database of glacial landforms and features related to the last British ice sheet. Boreas, 33, 359–375, 2004.

Bolikhovskaya, N. S.: Paleoenvironments and climato-stratigraphy of the loess-paleosol formation of Northern Eurasia. LOESSmFORM, 4, 11–36, 2004.

Faibusovic, Ya. E. and Abakumova L.A. Map of Pliocene-Quaternary formations. 3rd ed. Scale 1:1,000,000. Federal Agency for Subsoil Use (Rosnedra), Map Q-43 (New Urengoy.) St. Petersburg: VSEGEI Cartographic Factory, 2015.

Fredin, O., Rubensdotter L., Welden, A., Larsen, E. and Lysa, A.: Distribution of ice marginal moraines in NW Russian, Journal of Maps, 8(3), 236–241, 2012. doi: 10.1080/17445647.2012.708536

Glasser, N., Jansson, K., Harrison, S., and Kleman, J.: The glacial geology and Pleistocene history of South America between 38,8S and 56,8S. Quaternary Science Reviews, 27, 365–390, 2008.

Grosvald, M.G.: Eurasian Hydrospheric Catastrophes and Glaciations of the Arctic Region, Nauchny Mir, Moscow, 1999.

Groysman, Ya.M.: Geological survey of the Haigi-Yakh River basin (Long-Yugan). VSEGEI, Leningrad, 1954.

Generalov, P.P.: Upper Pleistocene of the lower course of the Ob River In: Collection of scientific papers of the West Siberian Scientific and Research Geological Prospecting Petroleum Institute, Tyumen, 56–77, 1986.

Immonen, N., Strand, K., Huusko, A., and Lunkka, J.P.: Imprint of late Pleistocene continental processes visible in ice-rafted grains from the central Arctic ocean. Quaternary Science Reviews 92, 133–139, 2014.

Interregional stratigraphic chart of the Quaternary of the territory of the Russian Federation. Interdepartmental Stratigraphic Committee, VSEGEI, St. Petersburg, 2014.

Kalinska-Nartisa E., Woronko B., and Ning Wenxin. Microtextural inheritance on quartz sand grains from Pleitocene periglacial environments of the Mazovian Lowland, Central Poland. Permafrost and Periglacial Processes 28, 741–756, 2017.

Khabakov, A.V.: On roundness indexes of pebble, Sovetskaya Geologiya, 10, 98–99, 1946.

Khlebnikov, V.I.: Geological and geomorphological survey of a part of the middle reaches of the Nadym river basin. VSEGEI, Leningrad, 1954.

Krinsley, D.H., and Doornkamp, J.C.: Atlas of quartz sand surface textures. 2nd edition. Cambridge, Cambridge University Press, 102, 2011.

Kind, N.V.: Late Quaternary Geochronology According to Isotope Data. Nauka, Moscow, 1974.

Lazukov, G.I.: Antopogen of the northern part of Western Siberia (Paleogeorgaphy), Moscow, 127 p, 1972.

Maslennikov, V.V.: Regional Geo-Ecological Mapping at Scale of 1:1000000 Within the North End of Tyumen Oblast. Labytnangi, 1998.

Molodkov, A.: The Late Pleistocene palaeoenvironmental evolution in Northern Eurasia through the prism of the mollusc shell-based ESR dating evidence. Quaternary International, (in press.), 2020.

Molodkov, A.: Cross-check of ihe dating results obtained by ESR and IR-OSL methods: implication for the Pleistocene palaeoenvironmental reconstructions. Quat. Geochronol., 10, 188–194, 2012.

Molodkov, A., and Bolikhovskaya, N.: Climato-chronostratigraphic framework of Pleistocene terrestrial and marine deposits of Northern Eurasia based on pollen, electron spin resonance,

and infrared optically stimulated luminescence analyses. Est. J.Earth Sci. 59(1), 49–62, 2010.

Molodkov, A., and Bitinas, A.: Sedimentary record and luminescence chronology of the Lateglacial and Holocene aeolian sediments in Lithuania. Boreas, 35 (2), 244–254, 2006. ~~Copernicus Open Access Hub (n.d.) Available at: https://scihub.copernicus.eu/dhus/#/home~~

Nazarov, D.V.: Upper Pleistocene in the northern end of Western Siberia. In: Fundamental problems of the Quaternary, results of the study and the main trends of further research: Proceeding of the IX All-Russian Conference on Quaternary Research, Sochava Institute of Geography of the SB RAS, Irkutsk, 323–325, 2015.

Norris, S. L., Margold, M,. and Froese, D.G.: Glacial landforms of northwest Saskatchewan. Journal of Maps, 13, 600–607, doi:10.1080/17445647.2017.1342212, 2017.

Rukhin, L.B.: Fundamentals of Lithology. Doctrine of Sedimentary Rocks. Nedra, Leningrad, 1969.

Rusakov, A., Sedov, S., Sheinkman, V., Dobrynin, D., Zinovyev, E., Trofimova, S. and Levchenko, S.: Late Pleistocene paleosols in the extra-glacial regions of Northwestern Eurasia: Pedogenesis, post-pedogenic transformation, paleoenvironmental inferences. Quaternary International. 501, 174-192, doi:10.1016/j.quaint.2018.03.020, 2018.

Sharpe, J., Sharpe, D., and Harris J.: A flowline map of glaciated Canada based on remote sensing data. Canadian Journal of Earth Sciences, 47, 89–101, 2010.

Sedov, S., Rusakov, A., Sheinkman, V., and Korkka, M.: MIS3 paleosols in the center-north of Eastern Europe and Western Siberia: Reductomorphic pedogenesis conditioned by permafrost? Catena, 146, 38–47, doi:10.1016/j.catena.2016.03.022, 2016

Sheinkman, V., Sedov, S., Shumilovskikh, L., Korkina, E., Korkin, S., Zinovyev, E. and Golyeva, A.: First results from the Late Pleistocene paleosols in northern Western Siberia: Implications for pedogenesis and landscape evolution at the end of MIS3. Quaternary International, 418, 132–146, doi:10.1016/j.quaint.2015.12.095, 2016.

Sizikova, A.O. and Zykina V.S.: The dynamics of the Late Pleistocene loess formation, Lozhok section, Ob loess Plateau, SW Siberia. Quaternary International, 365, 4–14, 2015.

Strelkov S.A., Saks V.N., Arkhipov S.A., Volkova V.S. The problem of the Quaternary glaciations of Siberia. The main problems of the study of the Quaternary period, Nauka, Moscow, 188–205, 1965.

Svendsen, J.I., Alexanderson, H., Astakhov, V.I., Demidov, I., Dowdeswell J.A., and Funder S.: Late Quaternary ice sheet history of Northern Eurasia. Quaternary Science Reviews, 23 (11-13), 1229–1271, 2004.

Sukhorukova, S.S., Kostyuk M.A., Podsosova, L.L., Babushkon A.E., Zolnikov, I.D., Abramova, S.A. and Goncharov, S.V.: Moraines and Dynamics of Glaciation in Western Siberia. Works of Institute of Geology and Geochemistry of the Siberian Branch of the USSR Academy of Sciences, Issue 672. Nauka, Novosibirsk, 1987.

~~The BRITICE Glacial Mapping Project: version two release, 2017. Available at: https://shefuni.maps.aregis.com/apps/webappviewer/index.html?id=fd78b03a74bb477e906 e5d4e0ba9abaf~~

Troitskiy, S.L. and Shumilova, E.V.: Stratigraphy and Mineralogical-Petrographic Peculiarities of Quaternary Deposits in the Vorontsov Yar Stratum in the Lower Course of the Yenisei River. In: Lithology and Conditions of Formation of the Quaternary Deposits of the Northern Eurasia, Institute of Geology and Geochemistry of the Siberian Branch of the USSR Academy of Sciences, Novosibirsk, 5–37, 1974.

Vasilyev, S.V.: Forest and Bog Landscapes of Western Siberia. Izdatelstvo NTL, Tomsk, 2007.

Velichko, A.A. and Timireva S.N.: Morphoscopy and morphometry of quartz grains from loess and buried soil layers, GeoJournal, 36(2/3), 143–149, 1995.

Velichko, A.A., Timireva, S.N., Kremenetski, K.V., McDonald, G.M. and Smith, L.C.: West Siberian Plain as a late glacial desert, Quaternary International, 237 (1-2), 45–53, 2011.

Velichko, A.A.: Current state of conceptions on continental glaciers of the Earth. Bulletin of the

896          Academy of Sciences of the USSR, Geographical Series, 3, 21–34, 1987.

897 Velichko, A.A., Konononv, V.M. and Faustova M.A.: The last glaciation of Earth: size and volume
898          of ice-sheets, Quaternary International, 41 (42), 43–51, 1997.

899 Vos, K., Vandenberghe, N. and Elesen, J.: Surface textural analysis of quartz grains by scanning
900          electron microscopy (SEM): From sample preparation to environmental interpretation,
901          Earth-Science Reviews, 128, 93–104, 2014.

902 Woronko, B.: Frost weathering versus glacial grinding in the micromorphology of quartz sand
903          grains: Process and geological implications. Sedimentary Geology, 335, 103–119, 2016.

904 Zemtsov, A.A.: Geomorphology of the West Siberian Plain (Northern and Central Parts),
905          Publishing house of the Tomsk State University, Tomsk, 1976.

906 Yevseyev, G.P., and Reynin, I.V.: Geological structure and geomorphology of the Tanlova, Right
907          Khetta, and Big Huhu basins (right tributaries of the middle segment of the Nadym river).
908          VNIGRI, Leningrad, 1958.

909 *Annexes*

910

911 Annex 1

912 Bulk content of chemical elements

| Sampling depth, m | Sample No | Bulk content, % | | | | | | | |
|---|---|---|---|---|---|---|---|---|---|
| | | $SiO_2$ | $Al_2O_3$ | $Fe_2O_3$ | $K_2O$ | $Na_2O$ | $P_2O_5$ | CaO | $TiO_2$ |
| K-1 | | | | | | | | | |
| 0.1 | S1 | 87.65 | 5.27 | 0.95 | 1.66 | 1.00 | 0.03 | 0.51 | 0.64 |
| 0.35 | S2 | 88.09 | 5.14 | 1.89 | 1.14 | 0.56 | 0.05 | 0.32 | 0.53 |
| 1 | S3 | 89.49 | 4.93 | 1.20 | 1.52 | 0.75 | 0.04 | 0.41 | 0.41 |
| 1.8 | S4 | 92.97 | 3.35 | 0.61 | 1.32 | 0.51 | 0.02 | 0.27 | 0.21 |
| 2.3 | S5 | 90.71 | 4.21 | 0.92 | 1.35 | 0.64 | 0.03 | 0.38 | 0.39 |
| 3 | S6 | 98.02 | 0.88 | 0.30 | 0.25 | 0.07 | 0.01 | 0.10 | 0.10 |
| 4 | S7 | 98.39 | 0.69 | 0.25 | 0.20 | <0.05 | 0.01 | 0.08 | 0.08 |
| NS-6 | | | | | | | | | |
| 0.3 | S1 | 90.60 | 6.20 | 0.87 | 0.91 | 0.63 | 0.08 | 0.28 | 0.37 |
| 0.7 | S2 | 91.85 | 4.57 | 0.74 | 1.47 | 0.58 | 0.01 | 0.41 | 0.37 |
| 1.4 | S3 | 93.22 | 3.92 | 0.51 | 1.15 | 0.57 | 0.01 | 0.31 | 0.25 |
| 3.2 | S4 | 92.37 | 4.05 | 0.75 | 1.38 | 0.62 | 0.02 | 0.43 | 0.35 |
| 4 | S5 | 90.32 | 5.39 | 0.98 | 1.74 | 0.62 | 0.02 | 0.46 | 0.47 |
| 4.2 | S6 | 97.33 | 1.54 | 0.26 | 0.15 | 0.45 | 0.00 | 0.18 | 0.08 |
| 4.6 | S7 | 89.79 | 5.86 | 0.95 | 1.80 | 0.65 | 0.03 | 0.63 | 0.35 |
| 5 | S8 | 96.65 | 1.88 | 0.28 | 0.42 | 0.49 | 0.01 | 0.20 | 0.11 |
| 7.4 | S9 | 97.29 | 1.46 | 0.24 | 0.25 | 0.48 | 0.01 | 0.16 | 0.07 |
| 9.2 | S10 | 97.78 | 1.19 | 0.21 | 0.07 | 0.45 | 0.01 | 0.17 | 0.07 |
| NS-13, 14 | | | | | | | | | |
| 1.1 | S1 | 97.72 | 1.43 | 0.21 | 0.00 | 0.43 | 0.00 | 0.14 | 0.10 |
| 3.1 | S2 | 91.00 | 1.26 | 5.62 | 0.00 | 0.63 | 1.28 | 0.16 | 0.07 |
| 3.5 | S3 | 96.58 | 1.22 | 1.14 | 0.15 | 0.56 | 0.12 | 0.18 | 0.11 |
| 4 | S4 | 98.14 | 0.99 | 0.15 | 0.00 | 0.48 | 0.00 | 0.15 | 0.07 |
| 4.3 | S5 | 96.25 | 1.18 | 1.58 | 0.07 | 0.47 | 0.06 | 0.16 | 0.24 |
| 4.75 | S6 | 92.75 | 1.23 | 5.08 | 0.01 | 0.64 | 0.02 | 0.18 | 0.12 |
| 5 | S7 | 98.34 | 0.89 | 0.17 | 0.00 | 0.43 | 0.00 | 0.13 | 0.09 |
| NS-20 | | | | | | | | | |
| 1.5 | S1 | 95.61 | 1.79 | 0.39 | 0.48 | 0.08 | 0.02 | 0.08 | 0.44 |
| 3.7 | S2 | 95.59 | 1.83 | 0.21 | 0.68 | 0.09 | 0.01 | 0.07 | 0.16 |
| 6.5 | S3 | 97.12 | 1.14 | 0.19 | 0.39 | 0.09 | 0.01 | 0.07 | 0.10 |
| 9.5 | S4 | 94.30 | 2.31 | 0.31 | 0.84 | 0.10 | 0.02 | 0.07 | 0.38 |
| 16.45 | S5 | 97.26 | 0.93 | 0.22 | 0.22 | 0.05 | 0.01 | 0.07 | 0.20 |
| NS-22 | | | | | | | | | |
| 1.1 | S1 | 96.49 | 1.53 | 0.32 | 0.61 | 0.17 | 0.01 | 0.11 | 0.17 |

913

914

915   Annex 2
916   Spearman's coefficients of correlation

|        | $SiO_2$ | $TiO_2$ | $Al_2O_3$ | $Fe_2O_3$ | MnO | MgO | CaO | $Na_2O$ | $K_2O$ | $P_2O_5$ | BaO |
|--------|------|------|-------|-------|------|------|------|------|------|------|------|
| $SiO_2$   | 1    | -1   | -1    | -0.89 | -0.84 | -0.76 | -0.89 | -0.89 | -0.79 | -0.81 | -0.62 |
| $TiO_2$   | -1   | 1    | 1     | 0.89  | 0.94 | 0.75 | 0.89 | 0.89 | 0.79 | 0.83 | 0.73 |
| $Al_2O_3$ | -1   | 1    | 1     | 0.89  | 0.94 | 0.78 | 0.89 | 0.89 | 0.79 | 0.84 | 0.73 |
| $Fe_2O_3$ | -0.89 | 0.89 | 0.89  | 1     | 0.93 | 0.95 | 0.75 | 0.75 | 0.61 | 0.97 | 0.61 |
| MnO    | -0.84 | 0.94 | 0.94  | 0.93  | 1    | 0.86 | 0.85 | 0.85 | 0.76 | 0.91 | 0.78 |
| MgO    | -0.76 | 0.78 | 0.78  | 0.95  | 0.86 | 1    | 0.67 | 0.67 | 0.52 | 0.99 | 0.54 |
| CaO    | -0.89 | 0.89 | 0.89  | 0.75  | 0.85 | 0.67 | 1    | 1    | 0.96 | 0.71 | 0.91 |
| $Na_2O$   | -0.89 | 0.89 | 0.89  | 0.75  | 0.85 | 0.67 | 1    | 1    | 0.96 | 0.71 | 0.91 |
| $K_2O$    | -0.79 | 0.79 | 0.79  | 0.61  | 0.76 | 0.52 | 0.96 | 0.96 | 1    | 0.56 | 0.96 |
| $P_2O_5$  | -0.81 | 0.83 | 0.84  | 0.97  | 0.91 | 0.99 | 0.71 | 0.71 | 0.56 | 1    | 0.59 |
| BaO    | -0.62 | 0.73 | 0.73  | 0.61  | 0.78 | 0.54 | 0.91 | 0.91 | 0.96 | 0.59 | 1    |

917   Significance level $p < 0.05$

918 Annex 3
919 Grain size distribution

| Sampling depth | Sample | Fraction size (mm) / Content (%) | | | | | |
|---|---|---|---|---|---|---|---|
| | | Silt and clay | Very fine sand | Fine sand | Medium grained sand | Coarse Sand | Very coarse sand |
| **K-1** | | *<0.09* | *0.125-0.09* | *0.25-0.125* | *0.5-0.25* | *1-0.5* | *>1* |
| 0.1 | S1 | 31.7 | 29.2 | 28.7 | 9.5 | 0.7 | 0.1 |
| 0.35 | S2 | 18.7 | 12.5 | 32.1 | 32.2 | 4.2 | 0.3 |
| 1 | S3 | 18.9 | 32.3 | 35.6 | 11.9 | 1.2 | 0.1 |
| 1.8 | S4 | 5.9 | 20.1 | 56.7 | 16.4 | 0.9 | 0.0 |
| 2.3 | S5 | 5.6 | 13.1 | 59.9 | 19.8 | 1.6 | 0.0 |
| 3 | S6 | 0.6 | 0.4 | 1.8 | 71.5 | 23.7 | 1.9 |
| 4 | S7 | 0.4 | 0.5 | 4.2 | 46.3 | 46.9 | 1.7 |
| **NS-6** | | *<0.075* | *0.10-0.075* | *0.25-0.125* | *0.5-0.25* | *1-0.5* | *>1* |
| 0.3 | S1 | 11.0 | 6.6 | 52.7 | 26.9 | 2.8 | 0.0 |
| 0.7 | S2 | 0.8 | 6.8 | 70.8 | 18.7 | 0.4 | 1.9 |
| 1.4 | S3 | 2.0 | 8.8 | 65.8 | 21.2 | 1.3 | 0.5 |
| 3.2 | S4 | 3.6 | 8.4 | 72.8 | 15.2 | 0.0 | 0.0 |
| 4 | S5 | 29.9 | 14.9 | 50.2 | 5.1 | 0.0 | 0.0 |
| 4.2 | S6 | 2.8 | 0.0 | 29.4 | 61.9 | 5.9 | 0.0 |
| 4.6 | S7 | 26.2 | 21.1 | 51.1 | 1.6 | 0.0 | 0.0 |
| 5 | S8 | 0.0 | 0.0 | 41.1 | 55.0 | 3.9 | 0.0 |
| 7.4 | S9 | 1.1 | 0.1 | 29.2 | 52.1 | 17.4 | 0.0 |
| 9.2 | S10 | 0.5 | 0.0 | 29.4 | 57.5 | 12.6 | 0.0 |
| **NS-13.14** | | *<0.075* | *0.10-0.075* | *0.25-0.125* | *0.5-0.25* | *1-0.5* | *>1* |
| 1.1 | S1 | 0.0 | 0.0 | 0.6 | 37.4 | 58.0 | 4.0 |
| 3.1 | S2 | 8.0 | 0.0 | 0.3 | 36.6 | 54.2 | 0.9 |
| 3.5 | S3 | 5.9 | 0.0 | 10.6 | 59.9 | 23.6 | 0.0 |
| 4 | S4 | 0.0 | 0.0 | 7.1 | 62.9 | 30.0 | 0.0 |
| 4.3 | S5 | 24.4 | 1.2 | 15.3 | 40.9 | 18.0 | 0.1 |
| 4.75 | S6 | 1.9 | 0.0 | 6.5 | 53.5 | 37.5 | 0.6 |
| 5 | S7 | 0.0 | 0.0 | 8.0 | 61.5 | 30.6 | 0.0 |
| **NS-20** | | *<0.09* | *0.125-0.09* | *0.25-0.125* | *0.5-0.25* | *1-0.5* | *>1* |
| 1.5 | S1 | 0.0 | 2.2 | 62.1 | 21.9 | 1.3 | 12.5 |
| 3.7 | S2 | 0.0 | 4.3 | 72.0 | 23.0 | 0.5 | 0.2 |
| 6.5 | S3 | 0.0 | 4.4 | 55.8 | 38.5 | 1.1 | 0.3 |
| 9.5 | S4 | 0.0 | 9.3 | 70.7 | 16.0 | 1.5 | 2.4 |
| 16.45 | S5 | 0.0 | 0.9 | 56.8 | 37.6 | 4.0 | 0.6 |
| **NS-22** | | *<0.09* | *0.125-0.09* | *0.25-0.125* | *0.5-0.25* | *1-0.5* | *>1* |
| 1.1 | S1 | 0.0 | 1.4 | 53.3 | 44.3 | 0.9 | 0.1 |

920
921
922
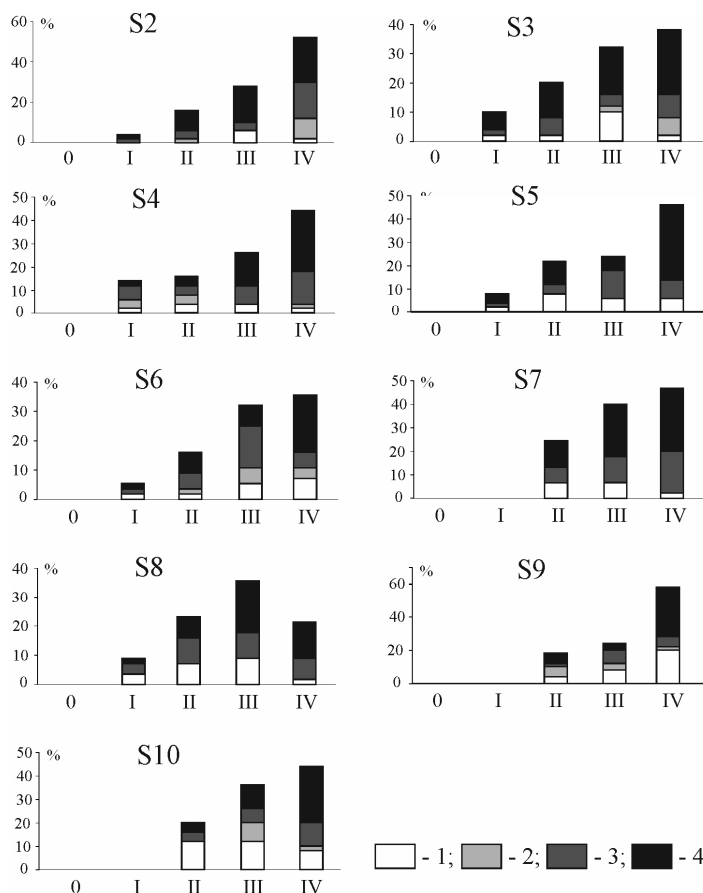
923
924     Annex 4. Distribution of quartz sand grains from section NS-6 by roundness and dullness.
925     1:glossy; 2:quater-matte; 3:half-matte; 4: matte; 0, I, II, III, IV are grades of roundness according
926     to Khabakov ~~seale~~ (1946)
927
928
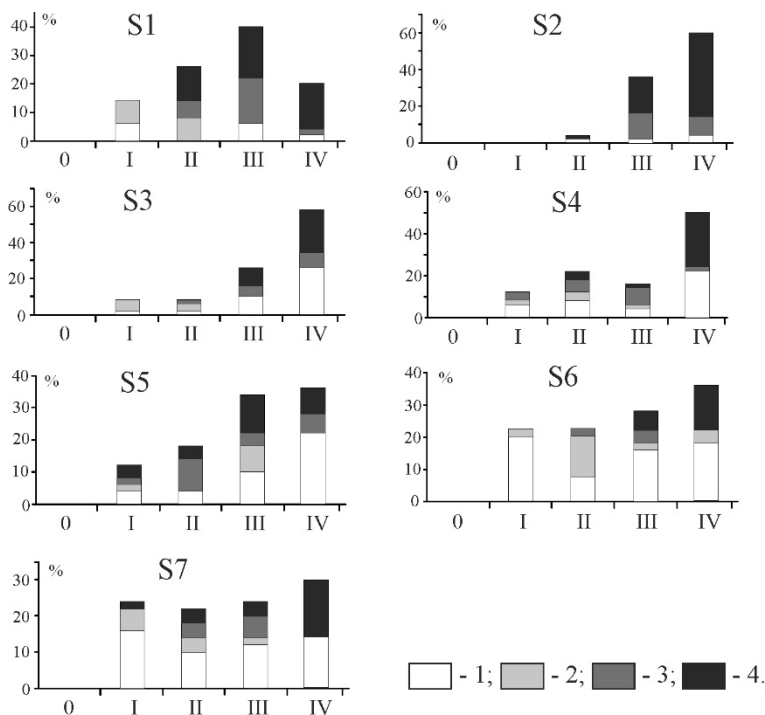
929
930     Annex 5. Distribution of quartz sand grains from section NS-6 by roundness and dullness.
931     1:glossy; 2:quater-matte; 3:half-matte; 4: matte; 0, I, II, III, IV are grades of roundness according
932     to Khabakov ~~seale~~ (1946)
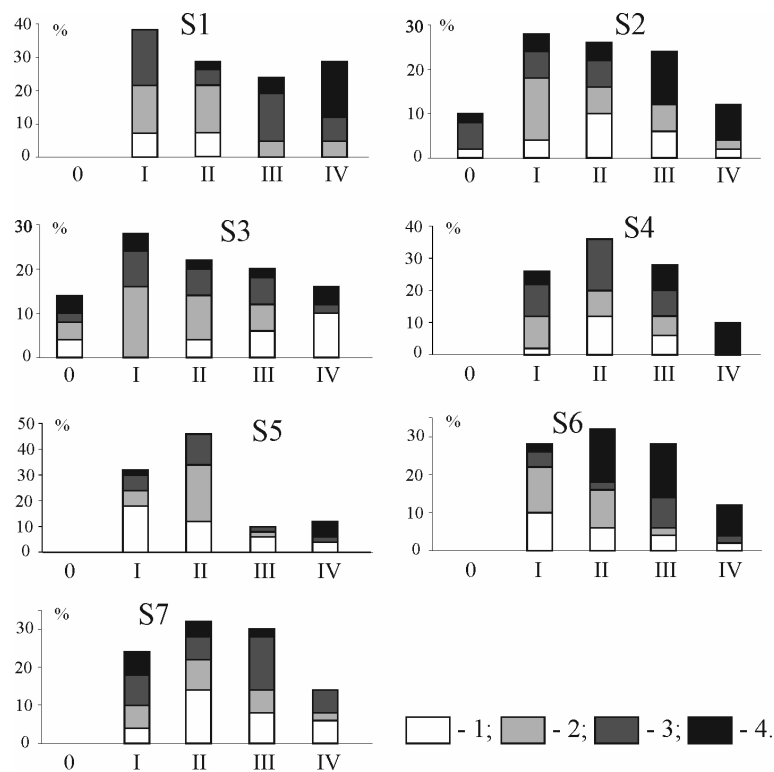
Annex 6. Distribution of quartz sand grains from section NS-13/14 by roundness and dullness.
935    1:glossy; 2:quater-matte; 3:half-matte; 4: matte; 0, I, II, III, IV are grades of roundness according
936    to Khabakov ~~scale~~ (1946)
937
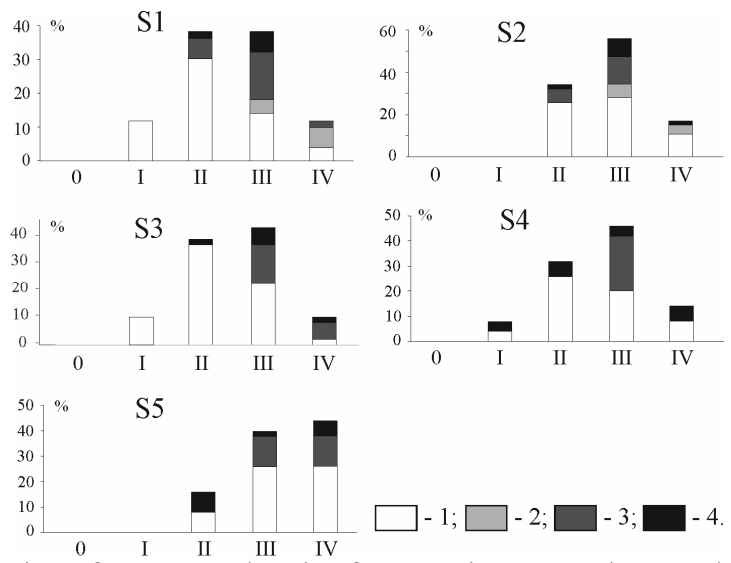
Annex 7. Distribution of quartz sand grains from section NS-20 by roundness and dullness.
940    1:glossy; 2:quater-matte; 3:half-matte; 4: matte; 0, I, II, III, IV are grades of roundness according
941    to Khabakov scale (1946)
942
943
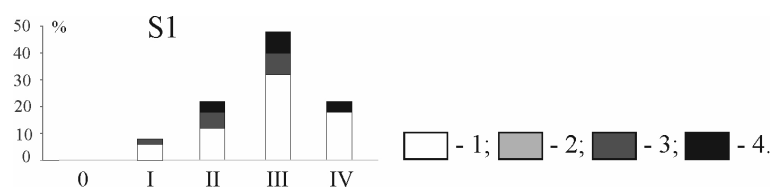
Annex 8. Distribution of quartz sand grains from section NS-22 by roundness and dullness.
946    1:glossy; 2:quater-matte; 3:half-matte; 4: matte; 0, I, II, III, IV are grades of roundness according
947    to Khabakov ~~scale~~ (1946)

948
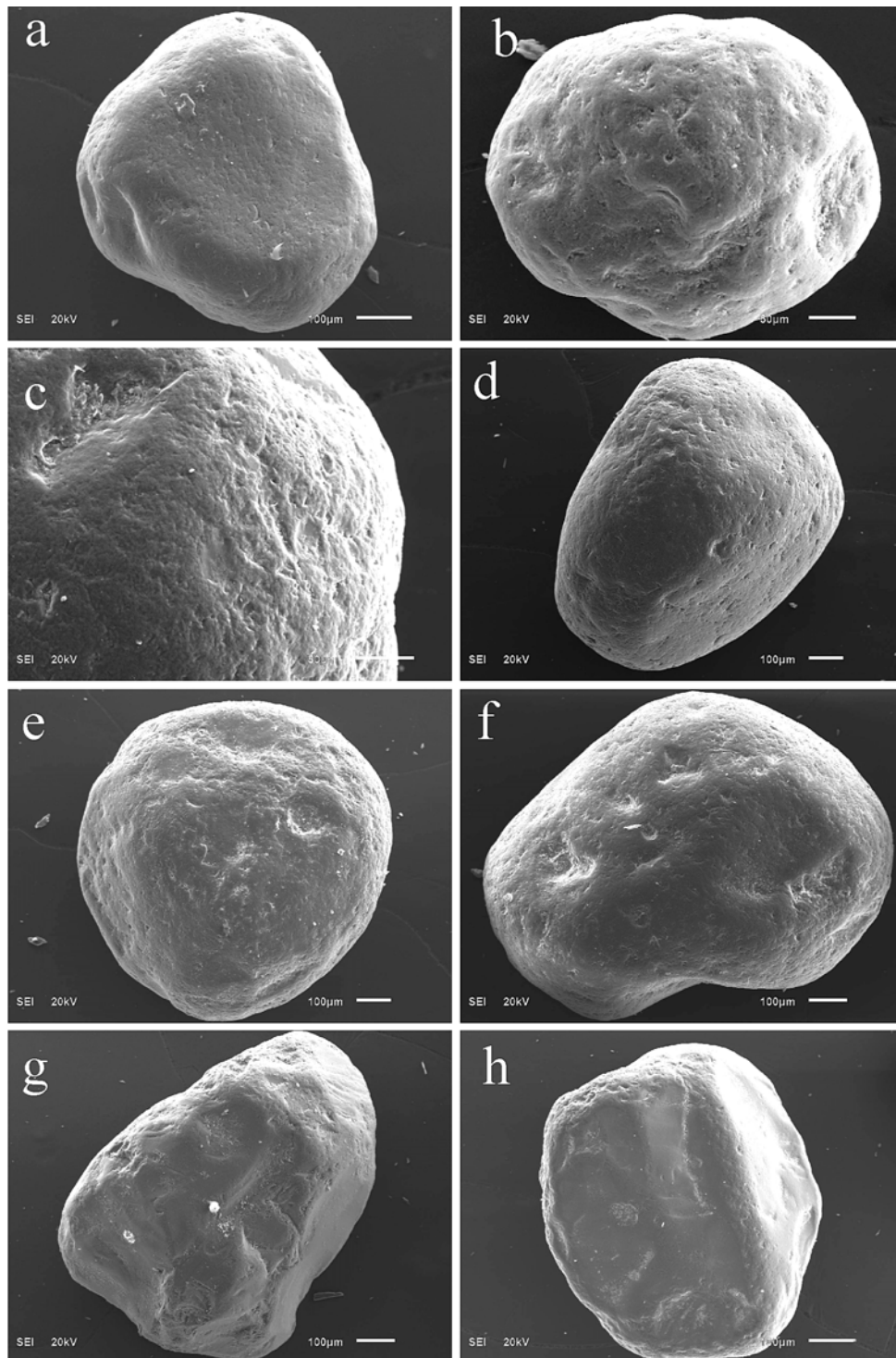
949
950
951 Annex 9. SEM photos of quartz grains, section NS-6.
952 Aeolian sediments: (a): dull grain with a micro-pitted surface and individual crescent-shaped
953 depressions, (b): matte grain with a micro-pitted surface and traces of previous subaquatic
954 treatment.
955 Floodplain sediments: (c): half-matte grain with V-shaped depressions, forming a fine-pitted
956 surface, and with micro-pits, (d): half-matte grain with V-shaped depressions and fine-pitted.
957 Fluvial deposits: (e): glossy grain with a fine-pitted surface; (f): half-matte grain with a fine-pitted
958 surface and separate V-shaped depressions; (g): glossy grain with fine-pits in the protruding parts
959 of the grain; (h): glossy grain with presedimentation fractures, with the surface subjected to aquatic
960 processes, as expressed by the shape of V-shaped depressions.
961

962
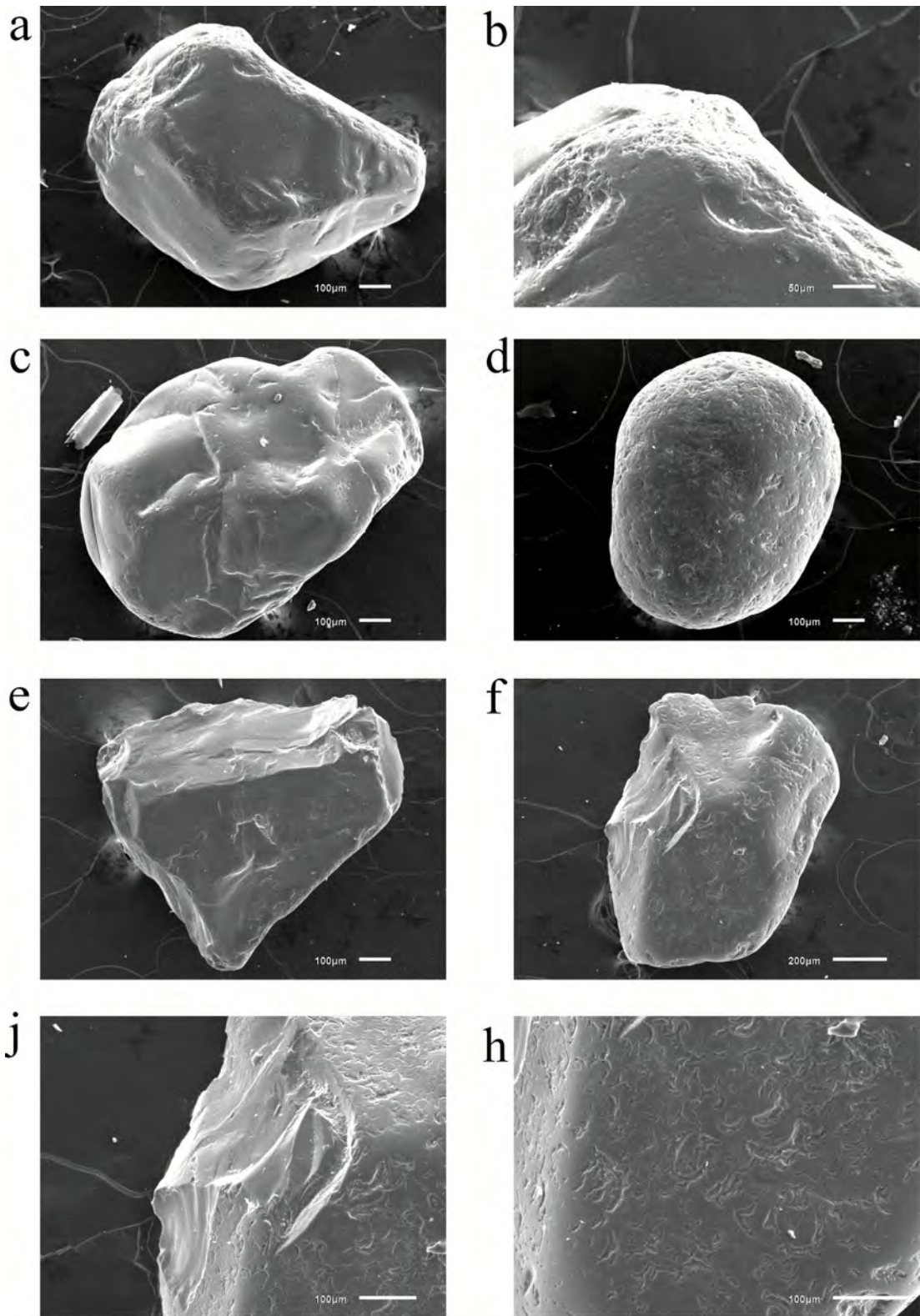
963
964 Annex 10. SEM photos of quartz grains from S7 section K-1: (a): glossy grain with a smooth
965 surface and flat faces; the faces feature crescentic pits, grain tops feature fine pits; (b): fine-pitted
966 surface of grain 'a'; (c): glossy grain with a smooth surface and sparse fine pits; (d): half-matte
967 grain with fine-pitted surface and crescent pits; (e): glossy grain with flat faces and no evident
968 texture; (f): glossy grain with post-sedimentation conchoidal fractures and crescentic pits;
969 (j):conchoidal fracture of grain 'e'; (h): crescentic texture of grain 'e'.
970
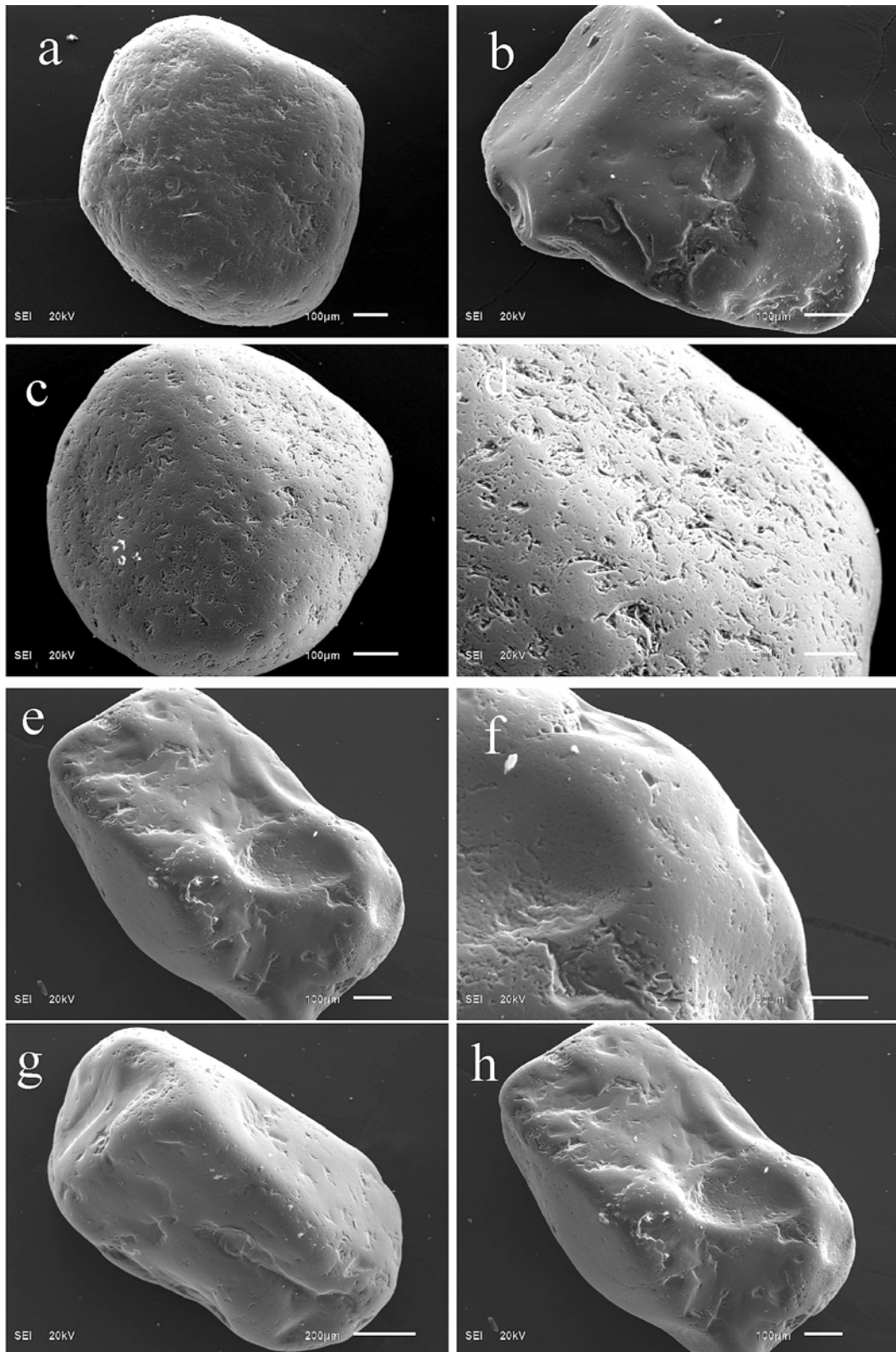
971
972 Annex 11. SEM photos of quartz grains from the section NS-13/14: (a) - glossy grain with fine-
973 pitted and crescent and V-depressions, (b): glossy grain of irregular shape with chips and
974 separate V-shaped recesses. Ns14: (c), (d): half-matte grain with a crescentic texture and
975 micropits; (e), (f): glossy grain with chips, V-shapes, and micro-pits on the protruding parts of
976 the grain; (g): half-matte grain of irregular shape with a fine-pitted texture in the protruding parts
977 of the grain; (h): glossy grain with a conchoidal fracture, V-shapes and fine-pits on the
978 protruding parts of the grain.
979
980

981
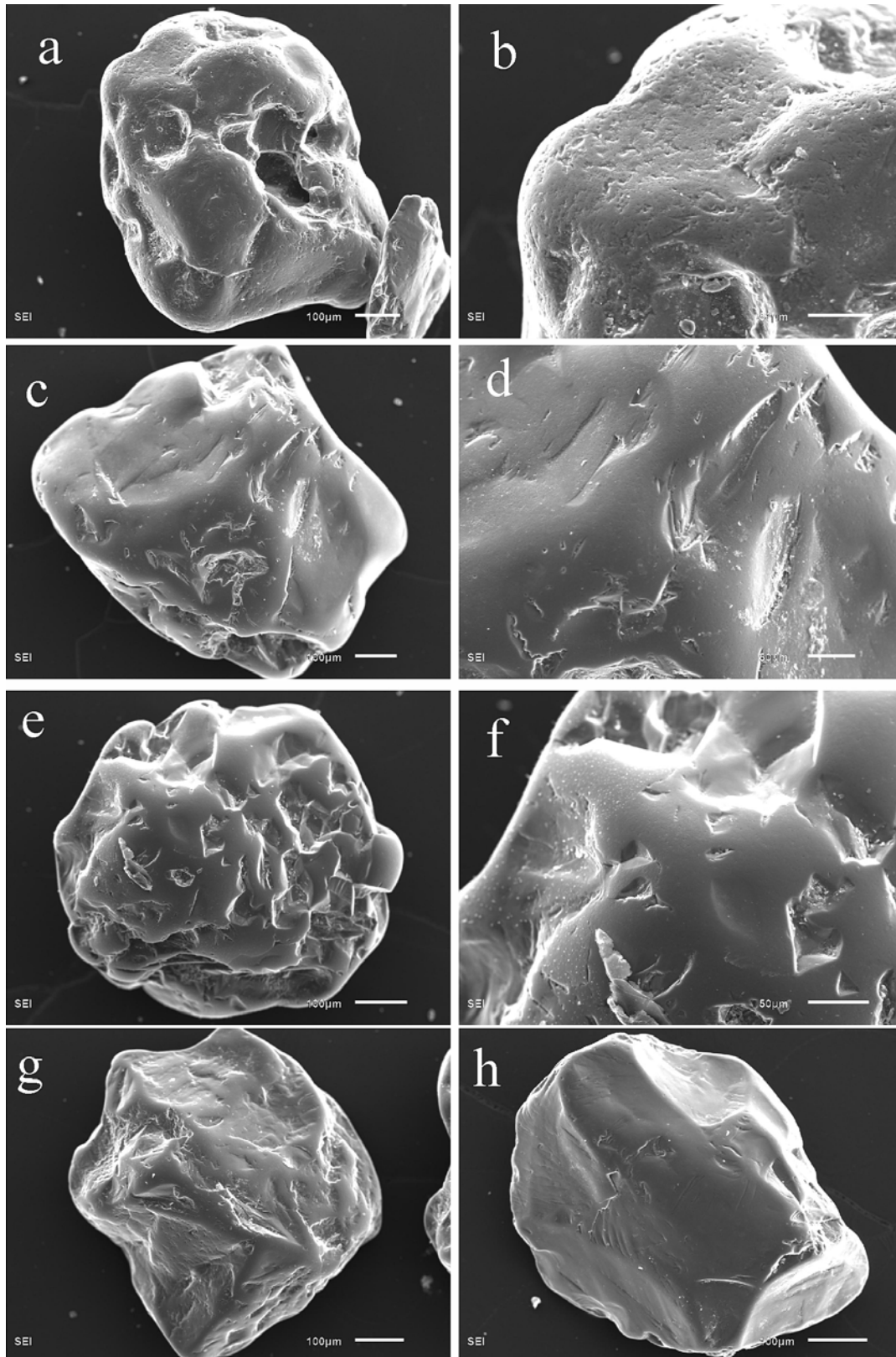
982
983 Annex 12. SEM photos of quartz grains from the section NS-20.
984 (a), (b): matte cavernous grain with a micro-pitted surface and individual crescentic and V-shaped
985 percussions, (c), (d): glossy grain with a smooth surface, grooves, and individual micro-pits, (e),
986 (f): glossy grain with deep groove and single V-shaped percussions, (g): glossy grain of irregular
987 shape with separate V-shaped percussions and a deep-pits, (h): glossy grain with presedimental
988 conchoidal fractures and scratches.
989
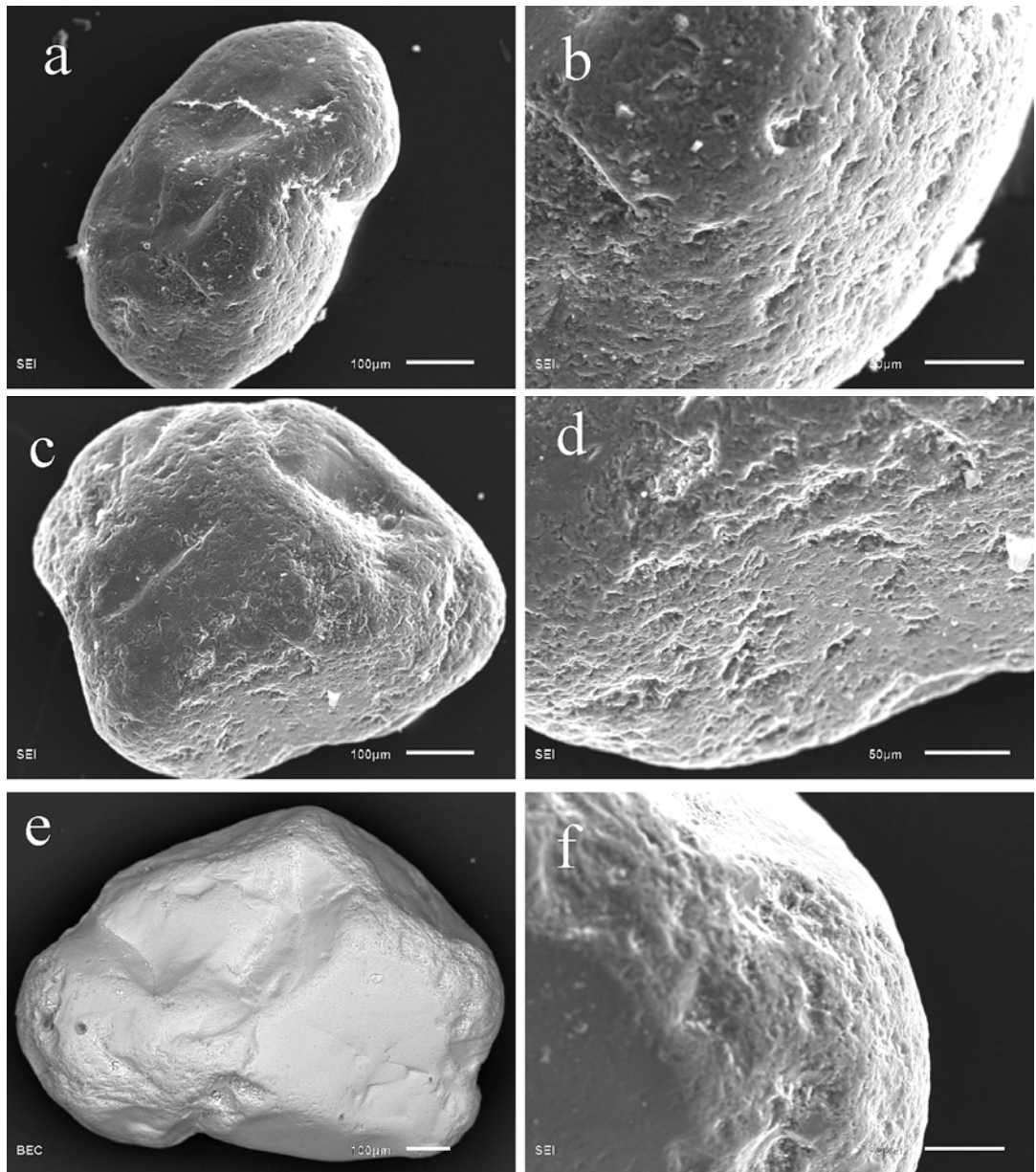
990
991 Annex 13. SEM photos of quartz grains from the section NS-22.
992 (a), (b): glossy grain with a fine-pitted surface, (c), (d): glossy grain with a fine-pitted surface,
993 (e), (f): glossy grain with fine-pits on the protruding parts of the grain.
994
995